AN ABSTRACT OF THE THESIS OF

Mitchell Alan Daniels for the degree of Master of Science in Mechanical Engineering presented on September 29, 2016.

Title: Experimental Classification of Intralaminar Matrix Compression Damage Propagation in Carbon Fiber Reinforced Polymers.

Abstract approved: _____

John P. Parmigiani

Composites often are able to carry more load after damage due to the structure of laminates. In addition, damage can be difficult to detect in composites compared to homogeneous materials. Understanding the behavior of composite material after damage is vital for composite structural design. Currently, experimental methods exist for classifying fiber tension, fiber compression, and matrix tensile damage propagation. However, little has been done on matrix compression propagation. First, several candidate specimens were identified based on fiber compression studies. These specimens were modeled using FEA and the base continuum damage mechanics models. The size of the matrix compressive damage region was compared to select the specimens. Compact compression and center notch compression specimens showed good isolation of compressive damage. Compact compression specimens were chosen, as they were less dependent on the boundary conditions to achieve the desired damage mechanisms. These specimens were then manufactured and tested along with uniform compression specimens. Shear cracks propagating through the thickness of the material were the primary failure mechanism observed,

with other damage mechanisms occurring after some propagation. A contour J-integral was used to measure the strain energy release rate from DIC displacement field data. The plastic behavior of the material was classified to determine the applicability of the J-integral. It was determined that the J-integral is potentially valid for compressive damage initiation. Typical values showed a range of energy dissipation values when damage initiation between 30 kJ/m^2 and 40 kJ/m^2. These values were reflected in the areas under the uniform compression specimen stress-displacement curves for similar fracture angles. These specimens also showed correlation between energy dissipation and fracture plane angle. This is due to a greater contribution of mode I compression at lower angles. Residual stresses were observed in the past damage material due to friction, fiber bridging and crack locking. These results show the limitations of the base continuum damage mechanics models and associated assumptions.

Experimental Classification of Intralaminar Matrix Compression Damage

Propagation in Carbon Fiber Reinforced Polymers

by

Mitchell Alan Daniels

A THESIS

submitted to

Oregon State University

in partial fulfillment of

the requirements for the

degree of

Master of Science

Presented September 29, 2016

Commencement June 2017

<u>Master of Science</u> thesis of <u>Mitchell Alan Daniels</u> presented on <u>September 29, 2016</u>

APPROVED:

_____

Major Professor, representing Mechanical Engineering

_____

Head of the School of Mechanical, Industrial, and Manufacturing Engineering

_____

Dean of the Graduate School

I understand that my thesis will become part of the permanent collection of Oregon State University libraries. My signature below authorizes release of my thesis to any reader upon request.

_____

Mitchell Alan Daniels, Author

ACKNOWLEDGEMENTS

CONTRIBUTION OF AUTHORS

Taylor Rawlings helped with support and presentation of chapter 2 and editing support for chapter 3. Dr. John Parmigiani provided guidance and feedback for chapters 2 and 3.

TABLE OF CONTENTS

TABLE OF CONTENTS

LIST OF FIGURES

LIST OF FIGURES (Continued)

LIST OF FIGURES (Continued)

LIST OF TABLES

NOMENCLATURE

Chapter 2

CNC   Center notched compression specimens

CC   Compact Compression

CT   Compact Tension

4PB   Four Point Bending

G Strain energy release rate due to damage input to continuum damage model

P Load inputted into specimen

C Compliance of specimen

a Length of damage region

Subscripts

m Property in the matrix or 90°

        direction

f Property in the fiber or 0° direction

t Tensile property

c Compressive Property

Chapter 3

E_1 Young's Modulus in the fiber direction

E_2 Young's Modulus in the matrix direction

σ_{ij} stress tensor

ε_{ij} Strain tensor

Γ contour around a region of damage

J J-integral value

w strain energy density

T_i traction vector

n_i normal vectors to Γ

u_i displacement vector

dS increment along contour Γ

A area of region enclosed by Γ

x horizontal direction parallel to the notch tip

y vertical coordinate perpendicular to x

CHAPTER 1: INTRODUCTION

The increased use of composite materials has lead the need to understand the

damage behavior of these materials. Understanding damage initiation and propagation is

important to mechanical design of load capacity and life of a component. Uncertainty in

damage behavior can lead to over conservative designs or premature failure of

components. Over conservative designs can be costly to produce and lead to inefficient

designs. Knowledge of damage progression is also a major part of certification and

design life. Damage progression is particularly important in composites because the load

transfer between the material components and the individual plies will often cause the

material to failure load to be much higher than the initial damage load. Despite its

widespread use there is still some uncertainty over modeling the mechanical behavior of

damage propagation in composites.

Damage in composite materials is complex due to the interaction of two dissimilar

materials leading to several different potential damage mechanisms. Damage mechanisms

in composites include fiber pullout, interface failure, fiber breaking/yielding, matrix

cracking/yielding, and delamination. In these materials, there are often several of these

damage mechanisms present in a damage region. This is a challenge when modelling the

effect of damage on the mechanical behavior as complex networks of damage

mechanisms are difficult to model explicitly. It is computationally prohibitive to

explicitly model each individual damage mechanisms and its effect on the macroscale

mechanical behavior.   A common method of modeling complex damage behavior is

continuum damage mechanics modeling. These methods have been implemented in FEA programs such as ABAQUS for simulating composite damage. Continuum damage mechanics models are advantageous because the overall effect of the damage is smeared across the entire damage region. This allows for the effect of damage to be modeled on the macroscale without explicitly modeling the damage mechanisms. The strain energy release rate due to damage is used as a material property input for the continuum damage mechanics model and governs the degradation of stiffness in damaged material. There are four strain energy release rates used in continuum damage mechanics of models for composite materials: fiber tension, fiber compression, matrix tension, and matrix compression. Uncertainty in these material model inputs can make simulations inaccurate and not representative of the physics of the material. For composites, the matrix compression energy is often the least understood and studied. The other three energy inputs have had extensive research on the classification of the damage behavior and measurement of the material input parameter.

This thesis focuses on experimentally classifying matrix compression damage mechanisms and damage propagation. Once the damage behavior is understood, improvements can be mode on the material models to increase their accuracy. First, relevant literature was reviewed. Then, a specimen selection study of candidate specimens was ran to select a specimen for isolating matrix compression damage. Once a specimen was selected, experimental tests were used to classify the mechanical behavior of matrix compression damage. The data was then used to calculate the energy dissipated due to a region of damage.

CHAPTER 2: SELECTION AND VALIDATION OF EXPERIMENTAL SPECIMENS FOR DETERMINING MODEL INPUTS FOR MATRIX COMPRESSION DAMAGE PROPAGATION IN FIBER REINFORCED COMPOSITES

2.1 Introduction

The increased use of composite materials across multiple industries, especially aerospace, has led to improvements of progressive damage models. These models require extensive knowledge of the damage mechanisms and material properties to accurately capture the physics of damage and the effects on the material. Continuum damage mechanics models use a strain energy release rate, or energy dissipated per area of crack growth, input to degrade the stiffness of damaged material. These types of models are commonly implemented in FEA programs, such as the commercial program ABAQUS [1]. The crack band theory is used to relieve the mesh dependence of energy dissipation rate [2]. Continuum damage mechanics models smear the properties of damage over the entire damaged region. This eliminates the need to model specific crack or damage geometry allowing for complex damage regions to be modeled fairly simply. For composite materials, there are four energy release rates representing different damage modes used as inputs for the continuum damage mechanics model; fiber tension, matrix tension, fiber compression and matrix compression. Extensive research has been done on the first three strain energy release rates resulting in effective experimental methods for determining their values. However, such methods do not exist for the matrix

compression strain energy release rate. It is often either assumed negligible or approximated from the mode II strain energy release rate and a fracture angle [3,4].

Several potential experimental specimens for the determining the matrix compression strain energy release rate are present in literature. They are based on studies focusing on fiber compression. In early studies, center notched compression (CNC) specimens were used [5-7]. CNC specimens for fiber compression are similar to specimens used in common composite compression tests such as the Boeing compression after impact test [8]. The center notch introduces a defect that initiatiates damage propagation in the specimens. Studies observed different failure modes from these specimens depending on notch orientation and the specimen layup. Failure modes observed included axial splitting, delamination, off-axis cracking and micro-buckling. Splitting perpendicular to the notch is often an undesired failure mode and prevents accurate measurement of other damage mode behavior. Sutlcliffe and Fleck [5] were able to mitigate this splitting with initiation sites for micro-buckling. However, Vaidya and Sun [6] still noticed splitting despite the use of initiation sites.

Compact Compression (CC) specimens are another commonly used specimen in fiber compression damage propagation studies which might be applicable to matrix compression [3,9,10]. These specimens are adapted from compact tension (CT) specimens outlined in the standard ASTM E399 [11]. CC specimens have similar geometry to CT specimens with a flared notch opening to prevent contact between the notch faces during loading. Studies showed fairly good isolation of fiber compression damage during damage initiation, but the strain energy release rate was observed to

increase as damage propagated. Pinho et al [3] noted that the increase in strain energy release rate was due to other damage modes present dissipating energy. It is also worth noting that Pinho et al [3] and Catalonotti et al [10] addressed matrix compression failure through assumptions in their studies. It was assumed that matrix compression strain energy release rate was negligible when compared to the fiber compression energy release rate in a cross ply laminate. It was also stated that the matrix compression damage can be represented as a single mode II crack in the 90 degree plies. They then subtracted the calculated matrix strain energy release rate out from the measured total energy release rate to isolate the fiber compression energy release rate.

Another specimen found in literature used to measure fiber compression strain energy release rate is the four-point bending (4PB) specimen [12,13]. Pinho et al [12] focused on manufacturing the specimens without producing distortion ahead of the crack tip. Laffan et al [13] were able to measure fiber compression propagation with 4PB specimens. In literature, 4PB specimens have shown some of the best isolation of fiber compression damage [14]. However, 4PB bending specimens as used isolate a slightly different failure mode from the specimens discussed previously, i.e. 4PB specimens isolate the through thickness fiber compression damage as compared to the intralaminar failure modes in CNC and CC specimens.

This study will focus on determing a specimen to isolate matrix compression damage to directly measure the matrix compression strain energy release rate experiementally. The process for selecting and validating a specimen for isolating matrix compression damage is outlined in this study. First, FEA models are created of the

candidate specimens to compare the size of the matrix compression damage region to determine damage isolation. A specimen is then selected and manufactured to be used in a preliminary experimental study to validate the damage isolation and concepts for measuring the strain energy release rate of the specimen.

2.2 Specimen Selection Study

2.2.1 General Methods

CNC, CC, and 4PB specimens were selected as candidate specimens for matrix compression damage isolation based on the literature covering fiber compression. To evaluate these candidates, FEA models were created of the specimens using the Abaqus built in continuum damage model for composite materials and an explicit solver. This model uses four strain energy release rate input parameters (Gmt, Gmc, Gft and Gfc) to linearly degrade the stiffness of a damaged element. Initiation of damage is governed by the Hashin failure model. The inputs were kept consistent across all models used in the study. Element deletion was not used in the models. Damaged elements were flagged and the stiffness was degraded according to the model. Continuum shell elements with eight nodes, SC8R, were used. Generally, one element through the thickness of the laminate was used, except for with 4PB specimens were each ply was modeled as a separate continuum shell element due to the orientation of the notch. Different plies were modeled when one element was used as integration points through the thickness. Each of the specimens consisted of twenty plies. For the CC and CNC specimens, the plies were oriented so the fibers were parallel to the notch tip, or 90 degrees to the load direction.

The plies in the 4PB specimens were oriented so the fiber direction ran parallel to the notch out-of-plane direction. Unidirectional layups such as all 0 degree plies and all 90 degree plies are rarely used in industry due to their high degree of anisotropy, but are useful for understanding and isolating specific damage modes. Boundary conditions were varied depending on the fixtures to be used with the specimens, but generally displacement boundary conditions were used.

2.2.2 CNC Specimen Methods and Results

The notch tip was initially modelled with a radius of 0.125 in for the CNC specimens modeled. A biased mesh with the finest mesh being 20 elements around the notch tip and a specimen length of 0.0023475 in was used. The coarsest mesh was at the corners of the specimen with an element size of around 0.17x0.16 in. Displacement boundary conditions were applied to the top and bottom edges of the specimens. The boundary conditions are shown in figure 1. The top edge was displaced 1 in in the negative y-direction and the bottom edge was held fixed. These boundary conditions were applied linearly over 8 seconds to simulate quasi-static conditions.
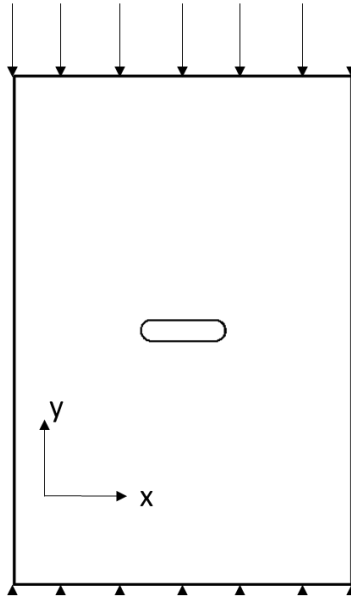
Figure 2-1: Displacement boundary conditions used in the FEA models of the CNC specimens

Two fixtures are commonly used with CNC specimens, edge mounted and face mounted. Initially, a face mounted fixture was modeled by constraining the out-of-plane displacement across the entire face of the specimen. The results from these models showed excessive splitting damage perpendicular to the notch tip. This is due to the boundary conditions preventing out-plane deformation forcing the material to expand parallel to the notch direction causing splitting damage instead of compressive crushing. To prevent this, an edge mounted fixture was modeled by constraining the out-of-plane displacement of the edges only, allowing out-of-plane displacement at the notch tip. A matrix compression damage region from a model of a CNC specimen is shown figure 2. In the figure, the light regions represent damaged material.
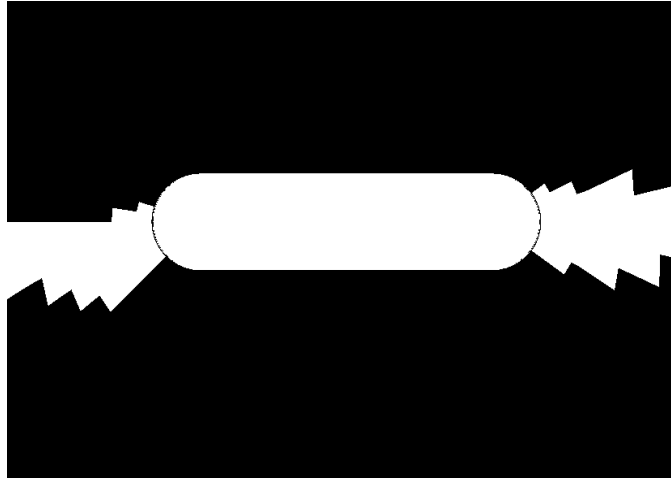
Figure 2-2: FEA results of an edge mounted CNC specimen. The light region represents damage and the dark represents undamaged material

Figure 2 shows damage matrix compression damage parallel to the notch. No other damage modes were present in this model besides matrix compression, showing the specimen failed as desired. The same damage region was present in all plies. This shows that surface damage tracking methods could potentially be used for these specimens, since the surface damage is representative of damage throughout the specimen. Models with a smaller notch tip radius (0.0625 in.) were created and showed similar results. Additionally, the layup was varied by adding some plies with fiber directions perpendicular to the notch tip. These models showed fiber compressive damage in conjunction with matrix compressive damage. Therefore, only unidirectional layups with all 90 degree plies will be considered moving forward with the other specimens.

2.2.3 CC Specimen Methods and Results

For CC specimens, two candidate geometries were chosen for the study; one with a sharp notch tip and one with a rounded notch tip (radius of 0.0625 in). Similar to the CNC models, the rounded notch models used a biased mesh with 20 elements around the notch

tip. Four elements were added between the notch tip and a partition with a notch radius of

0.125 in. A global seed of 0.05 in was used for the edges of the specimen. For the sharp

notch specimen, a biased mesh of 25 elements and a bias ratio of 5 was used between the

notch tip and the specimen edge. The largest elements were 0.11x0.625 in. at the

specimen corners. CC specimens use simple pin and clevis fixtures to load the specimen.

The fixtures were modeled as solid steel pins using continuum, 3-dimensional, 8 node,

reduced integration elements or C3D8R. Frictionless contact between the specimen pin

hole and the steel pins was used to load the specimens. Displacement boundary

conditions were applied to the pins. The boundary conditions are illustrated in figure 3.

A 1 inch displacement was applied in the negative y-direction to the upper pin and the

lower pin was fixed. The displacement occurred over 8 seconds to simulate quasi-static

conditions

Figure 2-3: Displacement boundary conditions used in the FEA models of the CC specimens

The damaged regions for the sharp and rounded notches are shown in figures 4 and 5

respectively. Similar to figure 2 the light regions represent damage in the specimen.
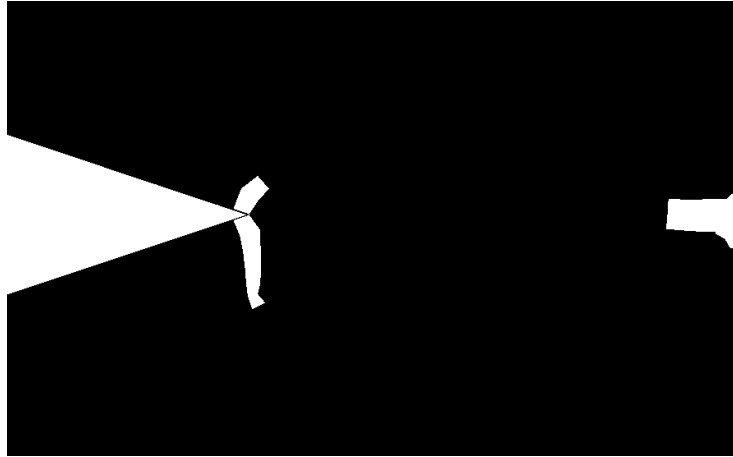
Figure 2-4: FEA results of a sharp notched CC specimen. The light region represents damage and the dark represents undamaged material
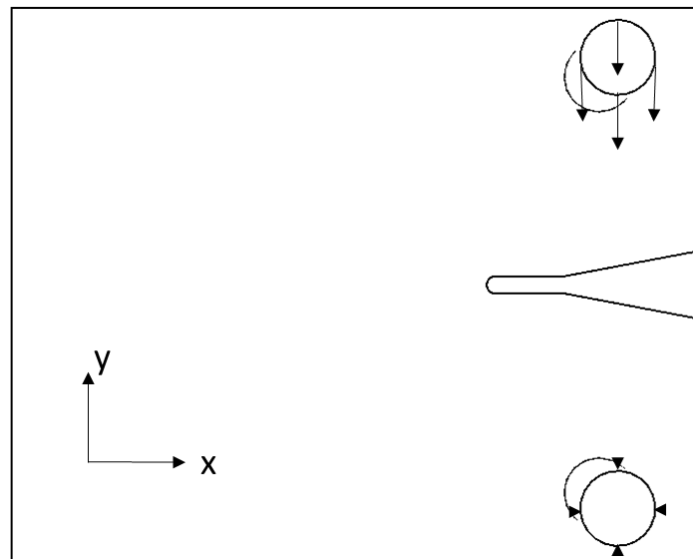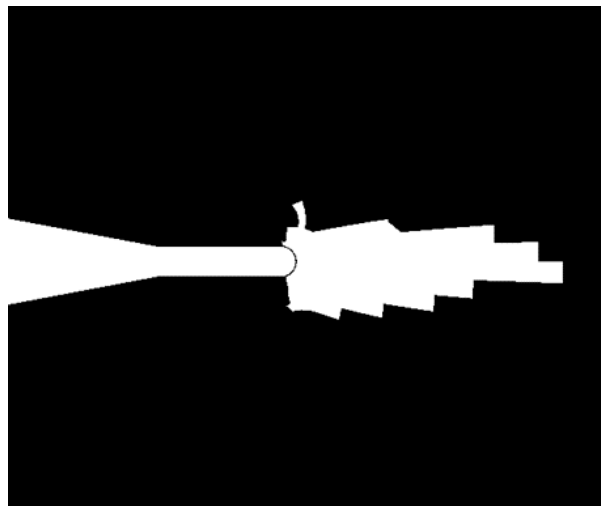

Figure 2-5: FEA results of a round notched CC specimen. The light region represents damage and the dark represents undamaged material

In figure 4, there is a small region of compressive damage at the notch tip with a larger

region of tensile damage at the opposite end of the specimen. The rounded notch

specimen in figure 5 was also prone to this type of tensile splitting, but only after a

significant amount of compressive damage had occurred. The damage region in figure 5

represents the matrix compressive damage region size before tensile splitting began to

occur. Careful design of the specimen geometry can delay the splitting mode to allow

more compressive damage growth.

2.2.4 4PB Specimen Methods and Results

4PB specimens were modeled with sharp notches. Continuum shell elements, SC8R,

were used to model each ply of the specimen. A biased mesh across the specimen with

the smallest elements set at 0.01 in and the largest at 0.1 in was used. Figure 6 shows the

4PB specimen geometry and the coordinate system used in the FEA models.
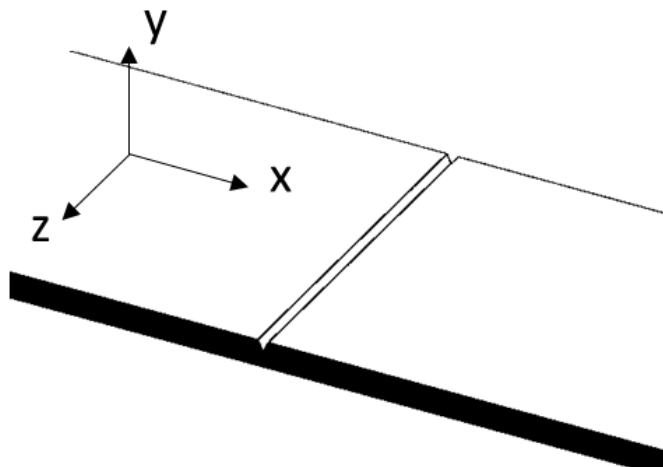
Figure 2-6: Sample 4PB geometry coordinate system. Displacement boundary conditions were applied in the y-direction and the fiber direction was in the z-direction

The fiber direction of the specimen was in the z-direction. The fixtures were modeled by

out-of-plane displacement boundary conditions applied in the y-direction along lines

parallel to the z direction. A displacement of 1 inch in the negative y-direction was

applied to the top of the specimen while the edges on the bottom side were remained

fixed. Rotations were remained free in order to prevent over constraining the specimen.

The results of a 4PB FEA model is shown in figure 7. The light region represents

damaged material.
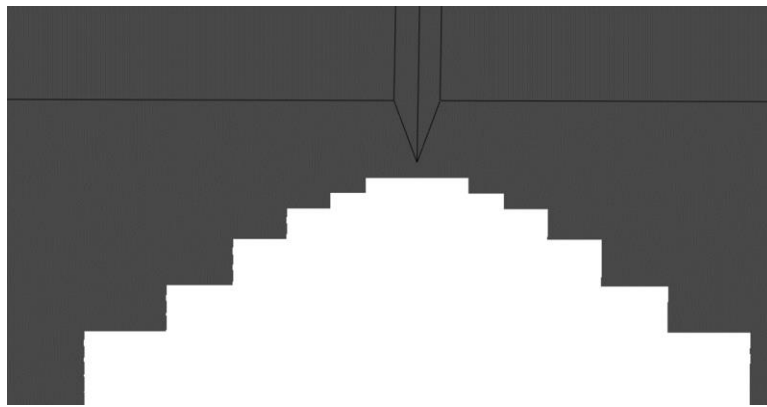
Figure 2-7: FEA results of a 4PB specimen. The light region represents damage and the dark represents undamaged material

The specimen modeled in figure 7 shows primarily matrix tension damage opposite of the

notch. This is due to a lower matrix tensile strength that the notch is not able to

overcome. Changes in geometry of the notch did not yield better results. Often times

similar failure modes would occur or the damage would shift to the loading points.

Matrix compression was not observed as the dominate failure mechanism for any of the

specimens modeled

2.2.5 Selected Specimen

CC specimens were selected to be pursued for testing based on the results of the initial FEA study. 4PB bending specimens were not able to isolate the desired failure modes with the geometries tested. Although CNC specimens showed fairly good isolation of compressive damage (roughly equivalent to CC specimens), the isolation was dependent on the boundary conditions applied. This translates to the specimens being dependent on the fixtures used. Compression instabilities require complex guards to prevent global buckling in the CNC specimens, but certain guards can force undesired failure modes. CC specimens require less complex fixtures for a similar specimen thickness. Therefore, CC specimens were chosen based on their simplicity and isolation of desired failure modes.

2.3   Experimental validation

2.3.1 Methods

Once the specimen geometry was selected, experimental tests were used to validate the base concepts for determining the matrix compression strain energy release rate and damage isolation of the specimen. CC specimens were manufactured using unidirectional pre-impregnated carbon fiber reinforced polymer. The specimens were cured at elevated temperatures in an oven using vacuum bags to apply mechanical pressure. Custom clevis pin fixtures were created with cutouts to allow for visual tracking of damage growth. The specimens were loaded in an Instron loading machine. Load and

displacement were recorded and the tests were filmed to track the surface damage to the specimen.

2.3.2 Results

Damage was clearly present on the surface of the specimen in the video of the tests. The progression of damage during loading is shown in figure 8.
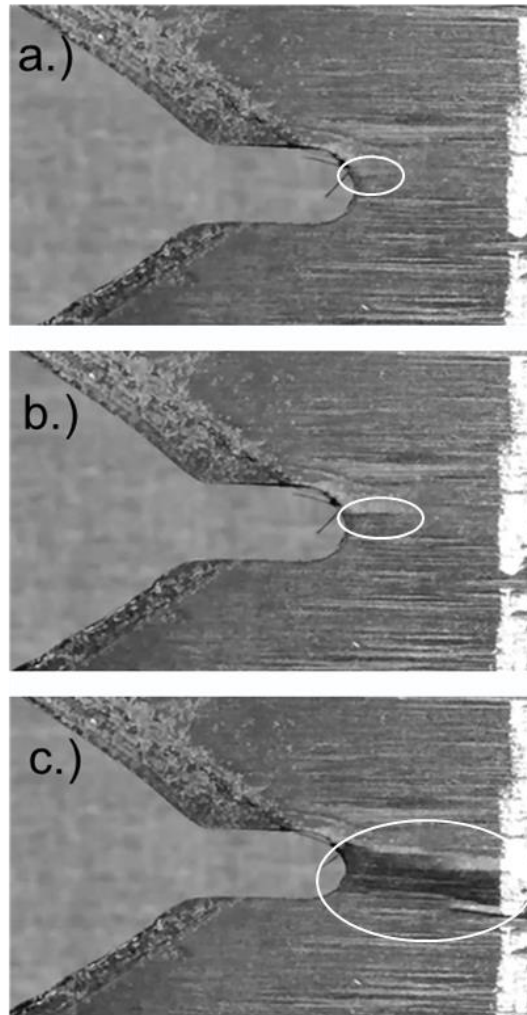
Figure 2-8: Visual damage progression of a CC specimen. a.) Damage initiation b.) Some damage progression c.)Large region of damage

The damage shown initiated at the notch tip and propagated outward showing good

isolation of compressive damage. The damage region size was measured using simple

image processing tools. Specimens with painted surfaces were tested to provide better

contrast between damaged and undamaged material, but the paint chipped before damage

of the specimen giving false damage region sizes. The main feature present in the damage

observed was bowing out of the specimen at the notch. An image of a specimen after

damage looking along the notch tip is shown in figure 9. The out-of-plane bowing of the notch tip is evident in this figure.
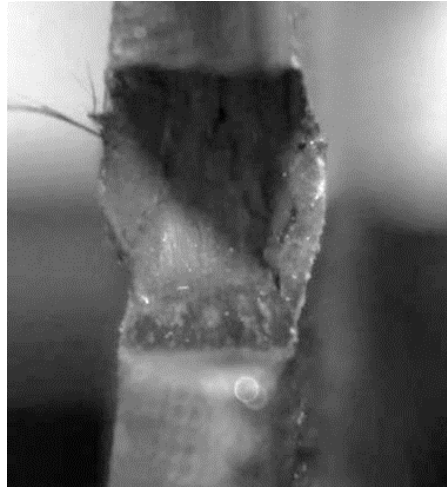
Figure 2-9: notch tip of specimen after damage showing out-of-plane bowing

It is worth noting that the ABAQUS model from the specimen selection predicted a similar bowing displacement. A view similar to figure 9 of the ABAQUS model is shown in figure 10.
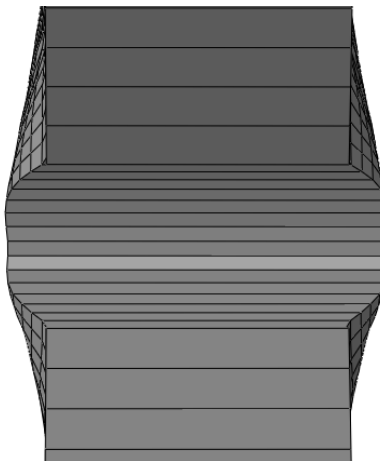
Figure 2-10: notch tip of Abaqus model of specimen after damage showing out-of-plane bowing

There are clear similarities in the displacements presented in figure 9 and 10. This suggests that the ABAQUS continuum damage model is able to predict some of the base damage mechanisms. The bowing is due to localized buckling. It is clear that it is separate from global buckling due to the symmetry of the damage. Generally, global buckling would have a tension and compression side on each face of the specimen. This suggests that the specimen isolated local compressive damage of the matrix. There is evidence of shear cracks and delamination in figure 9. Plastic deformation also appears to be present in the specimen as the notch tip largely remained in a deformed shape after unloading. With multiple damage modes present in the damage region, the question arises whether the damage shown classifies at pure matrix compression damage desired for the material model. This illustrates the importance of experimental classification of damage. Idealizing the damage to a pure constrained single damage mode in the matrix can decrease the accuracy of simulations and cause deviations from the actual physics of the damage behavior. Therefore, it is important to classify all the damage modes present in the material under the desired loading condition, e.g. compression of off-axis plies. The CC specimens show good isolation of compressive loading in the matrix, so it is desirable to consider all the damage modes in the potential material model. This is an advantage of continuum damage mechanics models, since the damage mechanisms are not explicitly modeled. Instead the overall effect of the damage on the material is modeled by degrading the stiffness. This allows for complex and multiple damage modes in the material to be modeled relatively simply, e.g. a large network of multiple cracks can be modeled as a single damage region instead of modeling each individual crack present.

The load displacement data from a representative test is shown in figure 11.
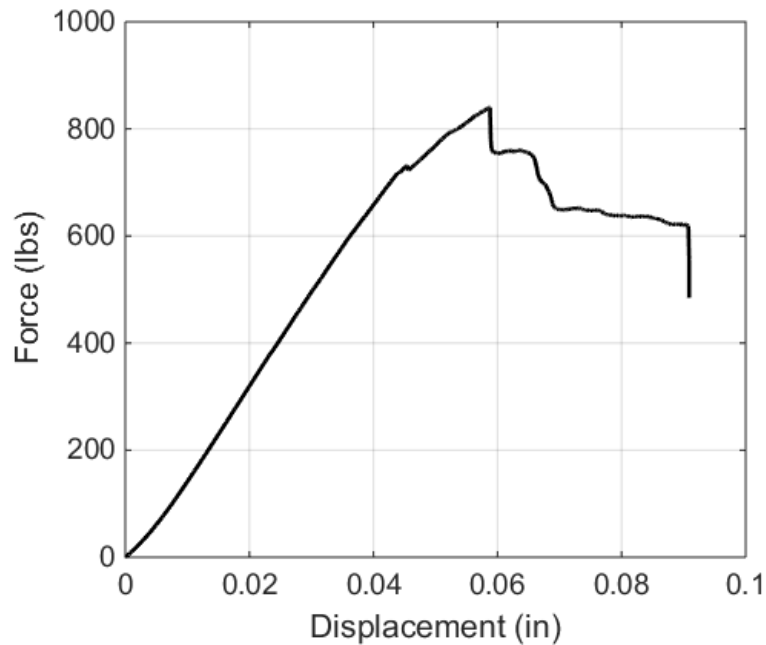
Figure 2-11: Representative load displacement curve from experimental tests of cc specimens

The load increases fairly linearly to a point, then appears to begin to show slight

nonlinearity before the load begins to drop off. This is consistent with the slight plasticity

observed in the damage region. The drops in load corresponded well with the increase in

damage region at the notch tip using time stamps from the data and video. This shows

that the load drops are due to compressive damage affecting the compliance of the

material. The load displacement curve was used to calculate the strain energy release rate

from the compliance calibration equation:

$$G = \frac{P^2}{2B}\frac{dC}{da}$$

From this equation, the strain energy release rate, G_{mc}, was calculated to be 35 in-lb/in^2. It is worth noting that this is a very rough value used as a proof of concept for the specimens. The compliance calibration method as implemented in the proof of concept tests relied on the displacement as measured by the Instron. This includes the compliance of the fixture as well as the specimen. The fixture compliance introduces error although it is relatively small compared to the specimen. In addition, the compliance calibration is valid for linear elastic fracture mechanics. If other damage modes are present besides elastic cracks, the calculated energy release from this method can be inaccurate. More refined data collection methods are required to provide an accurate value for input into the computational models. However, the calculated strain energy release rate is within the expected range. It is higher than reported values for matrix tension, as would be expected for compression as plasticity, crack turning, and material trapped in the damage region are expected to absorb additional energy.

2.4   Conclusions

FEA models were used to select a specimen for experimentally determining the matrix compression strain energy release rate. The built in ABAQUS continuum damage model was used to model compressive damage propagation of candidate specimens. Matrix compression damage region size was compared for each of the specimens. CC specimens were chosen based on their ability to isolate a large region of compression damage and relatively simple fixtures. The specimens were then created and tested. CC

specimens show promise for isolating matrix compression damage and measuring strain energy release rate inputs for continuum damage mechanics models. These specimens provide a direct way of experimentally determining the damage mechanisms and material model inputs. Direct experimental measurement is advantageous because it does not rely on idealizations or assumptions on the behavior of damage. The study presented here provides basic proof of concept validation for CC specimens as a method for measuring strain energy release rate of matrix compression. More refined techniques are required for data processing to provide an accurate energy dissipation due to damage. Overall, CC specimens showed good isolation of matrix compression damage.

2.5   References

[1] I. Lapczyk and J. A. Hurtado, "Progressive damage modeling in fiber-reinforced materials," *Composites Part A: Applied Science and Manufacturing,* vol. 38, pp. 2333-2341, 2007.

[2] Z. O. Bazant and B. Oh, "Crack band theory for the fracture of concrete," *Materials and Structures,* vol. 16, pp. 155-177, 1983.

[3] S. Pinho, P. Robinson and L. Ianucci, "Fracture toughness of the tensile and compressive fibre failure modes in laminated composite," *Composites Science and Technology,* vol. 66, pp. 2069-2079, 2006.

[4] A. Puck and H. Schurmann, "Failure analysis of FRP Laminates by means of physically based phenomenlogical models," *Composites Science and Technology,* vol. 58, pp. 1045-1067, 1998.

[5] N. Fleck, P. Jelf and P. curtis, "Compressive Failure of Laminated and Woven Composited," *Journal of Composites Technology and Reseach,* vol. 17, no. 3, pp. 212-220, 1995.

[6] R. S. Vaidya and C. Sun, "Fracture Criterion for Notched Thin Composite Laminates," *AIAA Journal,* vol. 35, no. 2, pp. 311-316, 1997.

[7] Y. Yeow, D. Morris and Y. Brinson, "A correlaive study between analysis and experiment on the fracture behavior of graphite/epoxy composites," *Journal of testing and evaluation,* vol. 7, no. 2, pp. 117-125, 1979.

[8] The Boeing Co., ""Advanced Composite Compression Tests", Boeing Specification Support Standard BSS 7260, Rev. C," The Boeing Co., Seattle Washington, 1988.

[9] J. Ratcliffe, W. Jackson and J. Schaff, "Compression Strength Prediction of Impact-Damaged Composite Sandwich Panels," in *60th Annual Forum Proceedings, American Helicopter Society*, Baltimore, 2004.

[10] G. Catalanotti, P. Cmanho, J. Xavier, C. Davila and A. Marques, "Measurement of resistance curves in the logitudinal failure of composites using digital image correlation," *Composites Science and Technology,* vol. 70, pp. 1986-1993, 2010.

[11] ASTM, *E399-06 Standard Test Method for Linear-Elastic Plane-Strain Fracture Toughness KIc of Metallic Materials,* 2006.

[12] S. Pinho, P. Robinson and I. Iannucci, "Developing a four point bend specimen to measure the mode I intrlaminar frature toughness of unidirection laminated composites," *Composites Science and Technology,* vol. 69, pp. 1303-1309, 2009.

[13] M. Laffan, S. Pinho, P. Robinson, L. Iannuci and A. McMillan, "Measurement of the fracture toughess associated with the longitudinal fibre compressive failure mode of laminated composites," *Composites: Part A,* vol. 43, pp. 1930-1938, 2012.

[14] M. Laffan, S. Pinho, P. Robinson and A. Mcmillan, "Translaminar fracture toughness testing of composites: A review," *Polymer Testing,* vol. 31, pp. 481-489, 2012.

CHAPTER 3:   EXPERIMENTAL CLASSIFICATION OF MATRIX COMPRESSION DAMAGE PROGRESSION MECHANISMS

3.1   Introduction & Literature Review

In recent years, significant advances have been made in progressive damage modeling of composite materials. The structure of composites often allow them to continue to carry load despite damage. Additionally composites can be easily damaged by tool drops or collisions and the structure can make detecting damage difficult. This makes damage progression modeling particularly important for the determining the safety of composite structures. Damage in composite materials can be grouped into four general categories: fiber tensile damage, matrix tensile damage, fiber compressive damage, and matrix compressive damage. Propagation behavior of the former three have been studied extensively using experimental techniques, while the latter is often driven by assumptions from initiation studies. A direct experimental approach for determining damage propagation is desirable due to the complexity of composite damage behaviors.

Many studies have proposed models for the behavior of the matrix under compressive loading and the initiation of damage. Fiber-microbuckling studies have shown plasticity and shear damage occur in the matrix when loaded in compression [1-6]. These studies also illustrate the importance of the matrix as it supports the fibers and governs the fiber compressive strength. Damage initiation models have shown that shear

damage is the dominate failure mode under transverse compressive loading [7-9]. Research has shown pure transverse compressive loading initiates as shear cracks through the thickness of the composite [9-11]. The cracks form a fracture plane at an angle >45°, usually around 53°±3° for many composite materials [9]. The angle is due to the compressive force working to close the shear crack forcing it to turn away from the max shear 45° failure plane to relieve some of the compressive crack closing force. The compressive force trends toward pure mode II loading of the crack as the angle approaches 90°.

Pinho et al. [12] assumed the energy release rate due to compressive damage in the matrix can be approximated from the mode II fracture toughness of the matrix. It was assumed that matrix compression damage is approximated as a single mode II crack in the 90° plies. From this assumption, the energy dissipated per area of damage growth can be calculated from the mode II energy release rate and the crack angle. The mode II assumption and the crack angle are based on the work in damage initiation under transverse compression. A fracture angle of 53° is often used for this calculation. Soutis and Curtis [6] used similar assumptions to subtract the matrix toughness values from the measured values of a cross ply laminate to get the fiber toughness values. Maimi et al [13] added a frictional term to the calculated strain energy release rate. The calculated strain energy release rates are often implemented in continuum damage mechanics models. Continuum damage mechanics models use energy dissipation to degrade the stiffness of a damage region. In these models, explicit damage mechanisms are not modeled as the stiffness degradation properties are smeared over the entire damage

region. The stiffness degradation is governed by a bilinear stress-displacement law, where the strain energy release rate is the area under the curve. These models are outlined for composite materials by Maimi et al [14] and Lapczyk and Hurtado [15] with the latter being implemented in the FEA program Abaqus. Both models use the crack band theory [16] to reduce the mesh dependency of the energy dissipated in an element.

Different specimens have been used to isolate compression damage in studies on fiber compression damage propagation. Earliest studies used center notched compression (CNC) specimens with varying degrees of damage isolation [17-19]. Modified versions of ASTM standard compact tension specimens [20] referred to as compact compression (CC) specimens have been employed to measure the strain energy release rate for fiber micro-buckling [12, 21, 22]. Four point bending (4PB) specimens are a third commonly used specimen in literature on fiber compression damage propagation [23, 24]. Laffan et al [25] noted that for fiber compression damage four point bend specimens have shown the fewest problems in isolating damage propagation.

Laffan et al [26] reviewed several data reduction methods for determining the damage strain energy release rate from common experimental methods. ASTM E399 [20] presents an equation for the strain energy release rate of a CT specimen. However, this equation was developed for isotropic metals and was shown to be inaccurate for orthotropic materials [12]. The area method is a simple data reduction scheme utilizing the area under the load displacement curve. Strain energy dissipation can be determined by the difference in area between to critical loads before and after a drop in load. The compliance calibration method uses the compliance change in the material and an

optically measured crack growth to determine the strain energy release rate. The modified

compliance calibration (MCC) method uses specimens with varying known notch lengths

to determine the change in stiffness with respect to crack length. This method is often

more accurate than the compliance calibration method because it does not rely on

optically measured crack growth [26]. However, the MCC method assumes a perfect

crack with zero residual strength, which may be inaccurate for compression. Numerically

calculating the J-integral is has been used to determine the energy release rate. The J-

integral can be calculated from FEA for a unit load for varying crack lengths to determine

a function of J-integral vs crack length that can be correlated to experimental [12] or it

can be determined from digital image correlation displacement fields [22].

Several data reduction methods rely on the tracking and measurement of the

damage region size. It is difficult to track compression damage accurately because it is

not as clear as tensile cracking. Most studies have used visual tracking methods such as

DIC [12, 22], shadow moiré interferometry [21], charge coupled device cameras [24],

and photoelastic coatings [19]. The disadvantage of these methods is that they only track

damage on the surface of the specimen: other methods have been developed to track

internal damage. X-ray radiography is a method to track internal damage that has been

implemented in some studies [18, 27, 28]. Acoustic emission sensors can also be used to

track internal damage [24]. There are two methods to track damage using acoustic

emission sensors. The first method uses a sensor to input sound waves into the material

and damage zones are measured by the change in reflection of these waves compared to

undamaged material. Pinho et al [12] used a similar method using ultrasonic C-scans to

measure the damage in a specimen after loading. The second method tracks damage based on the emission of sound waves created by damage energy dissipation. Electrical resistance has been used to track the progression of damage [29]. The resistance between two electrodes increases as damage progresses due to damage disrupting the continuity. Thermography has also been employed to tack damage energy dissipation in specimens [30]. As energy is dissipated, heat is released that can be measured using thermal imaging.

Extensive research has been done on classifying fiber compressive damage propagation behavior, but to the authors knowledge no such study exists for matrix compression damage. Matrix compression damage propagation parameters are often calculated using simplifying assumptions from the observed mechanisms in damage initiation studies. This calculation requires several tests to determine the fracture angle, the through mode II strain energy release rate, and the friction load between the crack faces. It is useful to have a direct method for experimentally determine the damage propagation behavior and strain energy release rate. This study will focus on classifying the matrix compression propagation behavior and determining the strain energy release rate from experimental specimens.

3.2   Methods

3.2.1 Experimental Set Up

3.2.1.1. Uniform Compression Specimens

Small rectangular uniform compression specimens were created to measure the effect of damage on the stress-displacement behavior. The stress-displacement curves are often used in damage mechanics models, and these specimens can be used to determine the base effect of damage. A range of specimens sizes were used to compare geometry dependence. The heights ranged from 11 mm to 18 mm with thicknesses of 3 mm and 4.4 mm. A representative specimen is shown in figure 3-1a. The height of each specimen was selected so buckling would not occur before compression damage. The uniform stress state allowing for stress behavior to be determined from load displacement data. Stress-displacement behavior is an important part of continuum damage models and determining the damage behavior.

The material used was commercially available TR50S/NB301 carbon fiber/epoxy composite manufactured by Mitsubishi Rayon. Large flat unidirectional plates were laid up on an aluminum sheet metal mold. Vacuum bags were used to apply mechanical pressure during the cure cycle to consolidate the plies and prevent void formation. Release film and peel ply were used to pull excess resin from the panel. The plates were cured in an oven with a ramp of 1.67°C/min and held at 135° C for 90 minutes. The fiber volume ratio of the pre-preg material is given as 60 percent. After the panels were cured and debagged, the plate faces were wet sanded to achieve a smooth finish. The specimens

were then cut from the larger panels. Vacuum bagging can often produce rounded edges where the bag conforms to the edges of the part. Cutting the specimen from larger panels allows for better quality edges and ensures more consistent thickness throughout the specimens. The edges were milled to ensure non-eccentric and uniform loading.

3.2.1.2. Compact Compression Specimens

In addition to the uniform compression specimens, it is desirable to identify a specimen that isolates the progression of compressive damage in a controlled way. This allows for the material behavior as the damage progresses to be measured. Specimens have been used in literature to isolate compression damage in composites. Three specimens were considered: CC, 4PB, and CNC. FEA models showed that CC and CNC specimens showed good isolation of matrix compression damage, while 4PB specimens showed primarily tensile damage [31]. CC specimens were selected because the specimens are much less reliant on the boundary conditions to achieve good isolation of compression damage.

Once the specimen type was determined, the geometry was varied in the FEA models to select the specimen dimensions by optimizing the compression damage region size. The geometry used for this is shown in figure 3-1b.
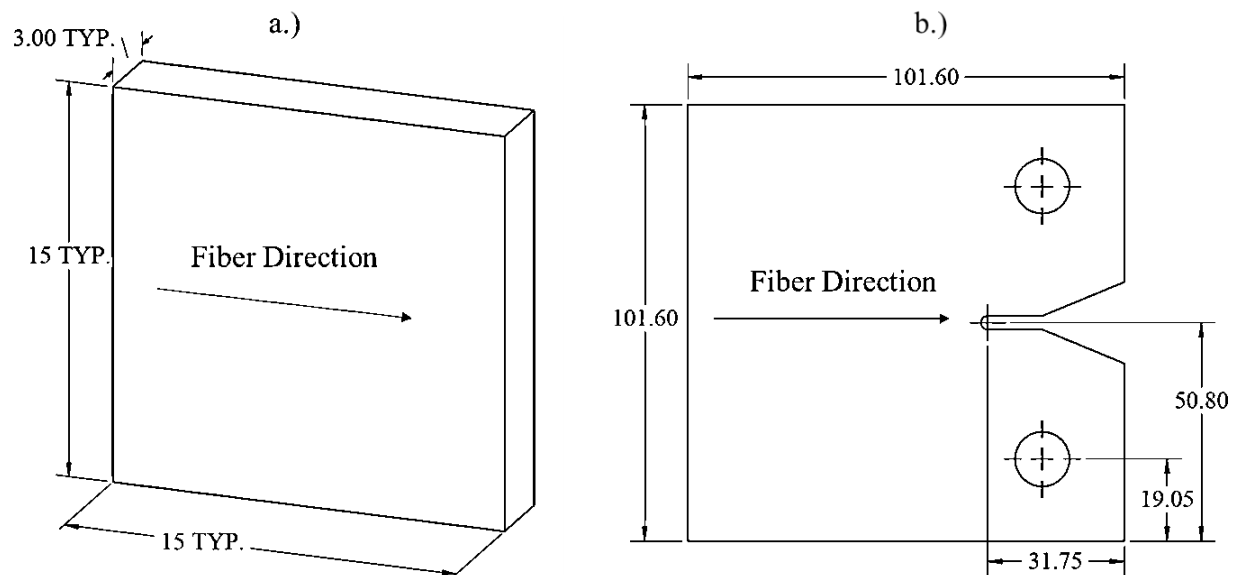
Figure 3-1: Geometry and fiber directions of a.) uniform compression specimens (representative) and b.) CC specimens. Dimensions are in mm

The opening of the specimen notch is flared to prevent the notch faces from contacting during loading. The fiber direction is parallel to the notch tip to isolate matrix compression damage at the notch, i.e. a layup schedule of $[90]_{25}$. Unidirectional layups are rarely used in industry, but are useful for isolating a specific property. A layup of twenty-five plies was determined to be sufficient for preventing global buckling of the specimen. Specimens were laid up using the same materials and methods as the uniform compression specimens. Manufacturing the specimens from a larger plate allows for more complex specimen geometry with better tolerances than from pre-cutting the material before layup. In comparison to rotary machining, waterjet cutting is less likely to cause delamination of the material in the specimen and is less hazardous to the operator.

3.2.1.3. Digital Image Correlation

Two firewire Point Grey Grasshopper Model GRAS-50S5M-C cameras were used for

the DIC data collection. The GRAS-50S5M-C is a monochromatic camera with

resolution of 2448x2048, a max frame rate of 15 FPS, a max transfer rate of 800 MBps,

and a 5MP Sony ICX625 sensor. A t-slot aluminum fixture was used to keep the cameras

focused on the specimen's region of interest. The fixture eliminates the need to

recalibrate the cameras during testing. The camera mount fixture is shown in figure 3-2.
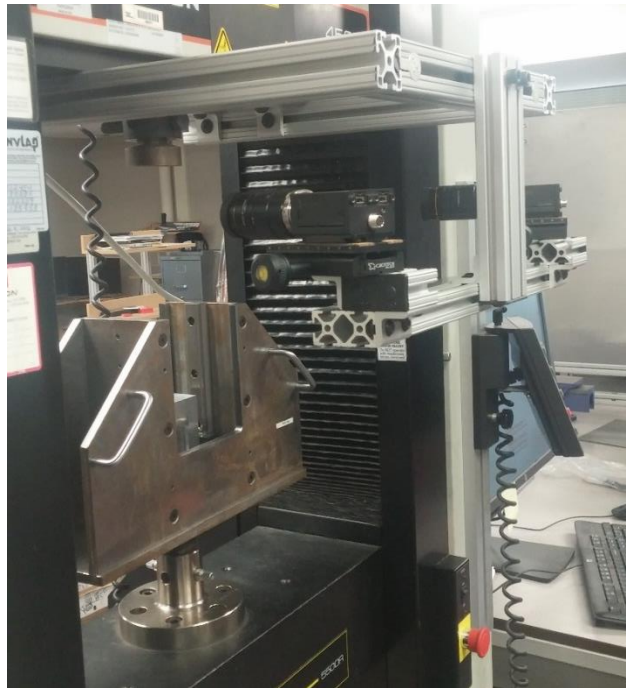
Figure 3-2: Camera Mount Fixture for DIC data collection

The fixture allows for the height of the cameras and the distance from the specimen to be

adjusted. The cameras were connected to a computer with a 2 channel IEEE 1394b PCIe

card. Labview with NI Vision Acquisition software was used to control the cameras.

DIC was used to measure the displacement and strain fields on the surface of the specimen. DIC measures displacement by tracking a subset in a pattern based on pixel values. It is desirable for the pattern used to be randomly distributed and high contrast. Spray paint was used to create the speckle on the CC specimens. Commonly specimens are painted white and then the speckle pattern is applied with black spray paint to increase the contrast of the pattern. Coating the specimen in paint may cause it to crack (especially under compression as the paint buckles) and give inaccurate damage regions. For this reason, white spray paint was applied directly to the composite material surface to create the speckle pattern. White spray paint provides a good contrast on the black surface of the carbon fiber specimen, but the reflectiveness of the surface does limit the contrast observed.

Two cameras were used to collect data so 3-D strain and displacement fields can be measured. Using stereoscopic effects, the two cameras are able to distinguish out of plane deformations increasing the accuracy of the displacement and strain fields as the out of plane deformation is no longer coupled with in plane deformations, e.g. hydrostatic expansion. Calibration was done using a 12x9 calibration grid with 2.5 mm spacing. The calibration grid is placed at the specimen location and images are collected at different grid orientations. Correlated Solutions' Vic-3D software was used to extract the information from the images and automatically calibrate the DIC set up for processing. The software automatically calculates the residuals of the images and displays the value in pixels. It is recommended that the correlation residuals be below 0.1 pixels with below 0.05 being ideal. For this study, 0.05 pixels was chosen as the threshold for an acceptable

correlation. The software automatically calculates and saves the camera properties so it the calibration can be imported for different data sets in the same session of testing.

3.2.2 Testing Plan

3.2.2.1. Uniform Compression Specimens

Testing was displacement controlled at a quasi-static rate of 0.1 mm/min. Monotonic loading tests were used to determine the total stress displacement behavior during and after damage. The tests were ended once the stress in the specimens dropped significantly. Unloading tests were used to classify the stress-strain behavior of the material before the onset of visible damage, i.e. the elastic and plastic response. Separate specimens were used for the monotonic and unloading tests so hysteresis in the unloading would not affect the monotonic stress-displacement behavior due to damage. Flat plate fixtures were used to load the specimens in pure transverse compression. A diagram of the loading fixture and specimen are shown in figure 3-3.
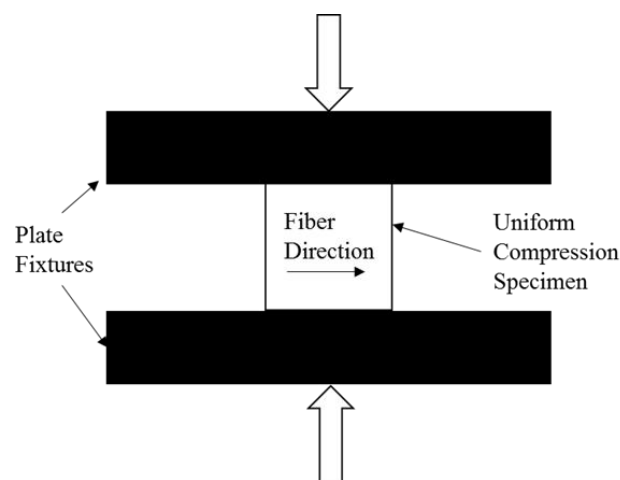
Figure 3-3: Loading and fixture diagram for uniform compression fixture testing

The load was recorded using an Instron 2525-810 load cell with a capacity of 6750 lbs and an uncertainty of 0.25% of the full scale range. The displacement data was measured using an extensometer. The strain and stress were calculated from the geometry of the specimen.

3.2.2.2. Compact Compression Specimens

The CC specimens were loaded at a displacement rate of 1 mm/min to achieve a quasi-static loading condition. Monotonic loading was used to understand the initiation and progression of matrix compression damage such as: damage region size, energy dissipation, and stiffness change. The monotonic loading cycle was also used to classify the damage mechanisms present in the material due to matrix compression loading.

Custom clevis pin fixtures were manufactured and are shown in figure 3-4. Steel was used for the loading fixture ensuring a significantly higher stiffness than the notched specimen. Custom fixtures were used to allow for DIC images to be captured during loading.

Figure 3-4: Custom pin and clevis fixture used to hold and load the specimens. The pins at the top were placed into the holes of the specimen and the bottom pins were in the load cell and load frame.

An Instron 2518-800 drop in load cell with a capacity of 100 kN and a repeatability of

0.25% was used to measure the load. The notch opening displacement was measured

using digital image correlation.

3.2.3 Analysis

3.2.3.1. DIC Fields

Displacement and strain fields were calculated from the speckle images using the

commercial software Vic-3D. Rigid motion was subtracted out of the data by applying

the average position transformation. Removing the rigid body motion ensures that only

the deformation of the part to be considered in the determination of the damage behavior.

A grid of points was created for further post processing. The displacement field from the

DIC software was used to calculate the notch opening displacement. Using DIC

eliminates error from the compliance of the fixtures in the displacement measurement, as

the displacement of the specimen is measured directly.

3.2.3.2. J-integral

Energy dissipation rate is a commonly used metric for damage growth models, such as

in continuum damage mechanics and fracture mechanics where the strain energy released

per surface area of a damage region is used. The J-integral [28] is a method of calculating

the strain energy release rate using a path independent contour integral for a path around

a crack and has been used to calculate the energy release rate of carbon fiber in

compression [19]. Although the basis of the J-integral is in fracture mechanics, it is

potentially valid for a region of compressive damage. Since the J-integral is derived from

the energy balance and a virtual crack extension, it should represent the damage strain

energy release rate provided there is not excessive plasticity, the damage region advances

in a regular manner, and the contour is sufficiently far from the damage region as to not

include plasticity. The J-integral may not represent the damage region stress singularity

as it does for fracture mechanics, since there are potentially more energy dissipation

mechanisms than simple cracks. The contour used for the J-integral calculation is shown

in figure 3-5. A simple rectangular contour is chosen to reduce the complexity of the

contour integral calculation.
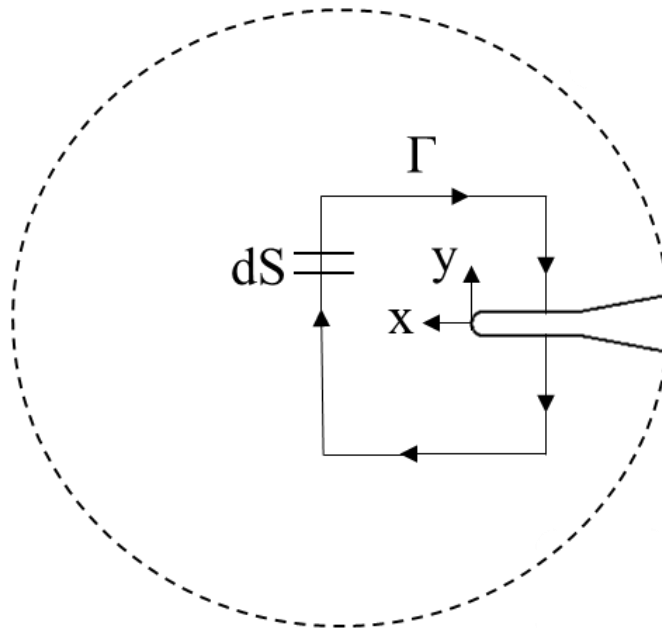
Figure 3-5: Section of specimen showing the contour path (Γ) around the notch used for J-integral calculations where dS is a differential section of Γ

The J-integral is evaluated along a contour path (Γ) by equation one using the horizontal and vertical coordinates, x and y, as shown in figure 3-5:

$$J= \int_{\Gamma} \left(w\,dy - T_i \frac{\partial u_i}{\partial x}\,dS\right) \tag{1}$$

Where u_i is the displacement vector, T_i is the traction vector and w is the strain energy density. The traction vector, T_i, is determined by:

$$T_i = \sigma_{ij} n_i \tag{2}$$

Where σ_{ij} is the stress tensor and n_j is the vector normal to the contour path. The strain energy density, w, is defined as:

$$w= \int_0^{\varepsilon_{ij}} \sigma_{ij} d\varepsilon_{ij} \qquad (3)$$

Where ε_{ij} is the strain vector. The J-integral is applicable for both linear elastic fracture

mechanics (LEFM) and elastic-plastic fracture mechanics. A program was created to

post-process the DIC data and calculate the J-integral. The program was verified by

comparing the J-integral calculation to the built in Abaqus J-integral in an FEA model.

The results of the validation are in shown table 3-1.

Table 3-1: Comparison of J-integral calculations between Abaqus and a custom post processing integral

Displacement (in)	Abaqus J-integral	Post-Processing Contour Integral	%Difference
0.1	-0.126	-0.13	-3.66
0.2	-0.505	-0.52	-3.63
0.3	-1.137	-1.18	-3.59
0.4	-2.022	-2.09	-3.54
0.5	-3.159	-3.27	-3.48
0.6	-4.549	-4.70	-3.40
0.7	-6.191	-6.40	-3.32
0.8	-8.087	-8.35	-3.22
0.9	-10.235	-10.55	-3.13
1	-12.635	-13.02	-3.03

A difference of less than 4% was deemed acceptable for the post processing code due to

coarse, irregular mesh used in the FEA model along the selected contour. In the post

processing of the DIC data, a finer mesh was used along a simpler contour to increase the

calculated J-integral accuracy. A finer mesh is more accurate because it decreases the

step size used in the numerical calculations trending the numerical value more toward the

actual derivative.

3.2.3.3. Damage Tracking

It is of interest to track the leading edge of the region of damage. Discontinuities in the displacement field were used to determine the location of the leading edge of damage. The method used was based on the work of Catalanotti et al [19]. In this method, the displacement discontinuity in an element is calculated from the difference in displacement values between nodes. The max difference in nodal displacement for an element is used as the discontinuity value for that element. This value is then compared to the average discontinuity of all the elements in the specimen and multiplied by a constant to create a threshold. Displacement discontinuity is used because damage, such as a crack, will create a large jump in displacement that is much greater than the displacement caused be the material deformation under load. Equation four shows a mathematical representation of this method. A script was used to post process the DIC data. Data points were grouped into elements and numbered within the elements as nodes with an integration point (IP) in the center. The element designation and coordinate system is illustrated in figure 3-6.
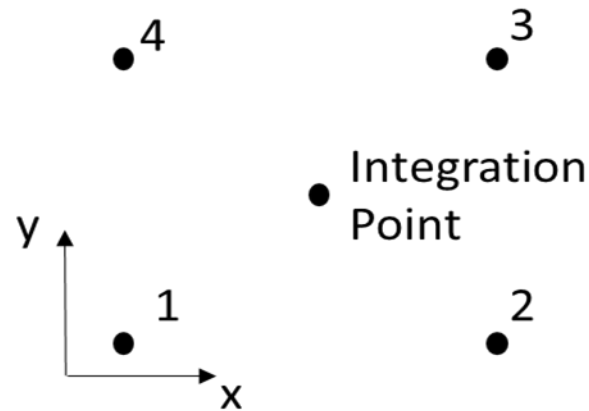
Figure 3-6: Element designation and coordinate system used to determine the displacement discontinuities.

The displacement discontinuity function at the integration point (Dis(IP)) in an element was determined from the maximum difference between displacements of the opposite corners of the element:

$$\text{Dis(IP)} = \max(\|u_i(4)\text{-}u_i(2)\|, \|u_i(3)\text{-}u_i(1)\|) \tag{4}$$

The value of the discontinuity function was compared to a threshold value of twice the discontinuity function mean. If the function is greater than the threshold value, it is given a value of one, else it is given a value of zero. The damage zone length is determined by the largest x coordinate of an integration point with a discontinuity function value of one.

3.3   Results and Discussion

3.3.1 Uniform Compression Specimens

3.3.1.1. Damage Mechanisms

The uniform compression specimens showed similar mechanisms to those predicted by work on damage initiation due to transverse compression loading [1, 2, 3]. Shear cracks formed at the specimen surface and progressed through the thickness direction at an angle. An example of a shear crack is shown in figure 3-7.
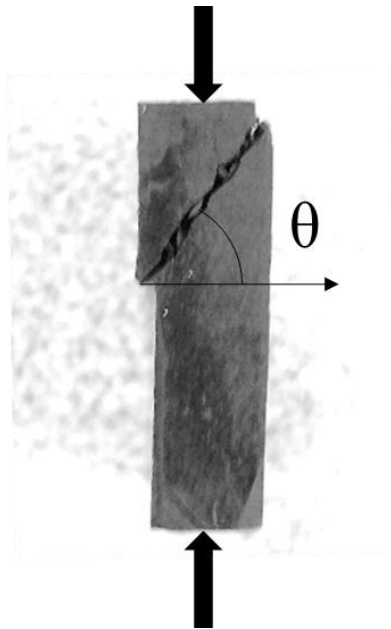
Figure 3-7: Shear crack through the thickness of a uniform compression specimen

Figure 3-7 shows a crack that propagated through the entire thickness of the specimen. There is evidence of material trapped in the wake of the crack due to fiber bridging and slight variations in the crack path. These mechanisms can lead to increase in energy absorption due to damage. A wide variety of fracture plane angles were observed in the

specimens ranging from 52° to 73°. The variation in fracture plane was potentially due to geometry differences creating slightly different stress states, e.g. bending leading to more shear loading, or due to manufacturing defects forcing the fracture in a certain direction.

3.3.1.2. Stress Displacement Curves and Energy Release

Uniform compression specimens were used to classify the stress displacement behavior. These specimens will create a uniform compression stress. Uniform compression specimens can simulate elements to determine the stress-displacement relationship to inform computational models. The stress displacement data for a few representative specimens are shown in figure 3-8 to illustrate the range of behavior. All other specimens tested showed similar behaviors to the curves in figure 3-8.
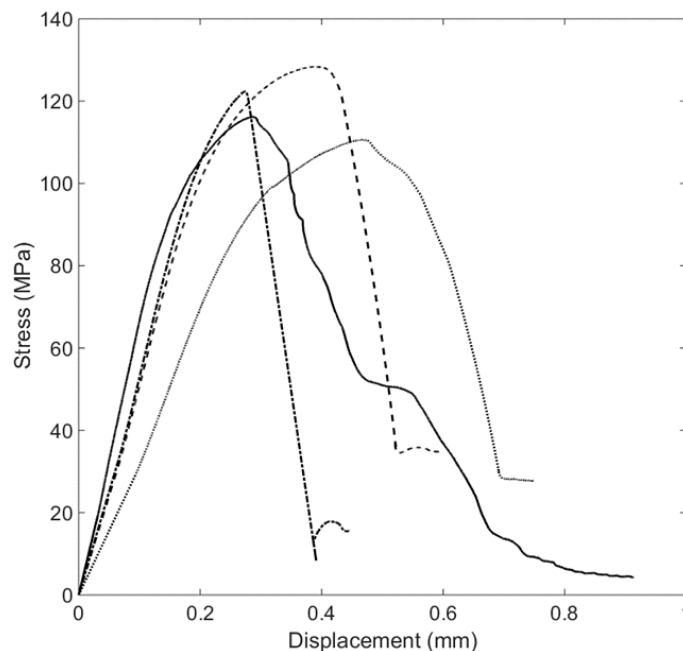
Figure 3-8: Stress displacement behavior of representative uniform compression specimens

Figure 3-8 shows a wide variety of displacement values at failure. This is due to the different dimensions of the specimens. Fracture often occurred quickly causing a sudden linear decrease in stress. This is a similar mechanism predicted from the continuum damage mechanics models. Some specimens showed a slower advancement of damage correlating with the progression of damage across the specimen instead of a sudden failure of the entire specimen.

The stress-displacement behavior can be split into regions to describe the behavior, as shown in the representative curve in figure 3-9.
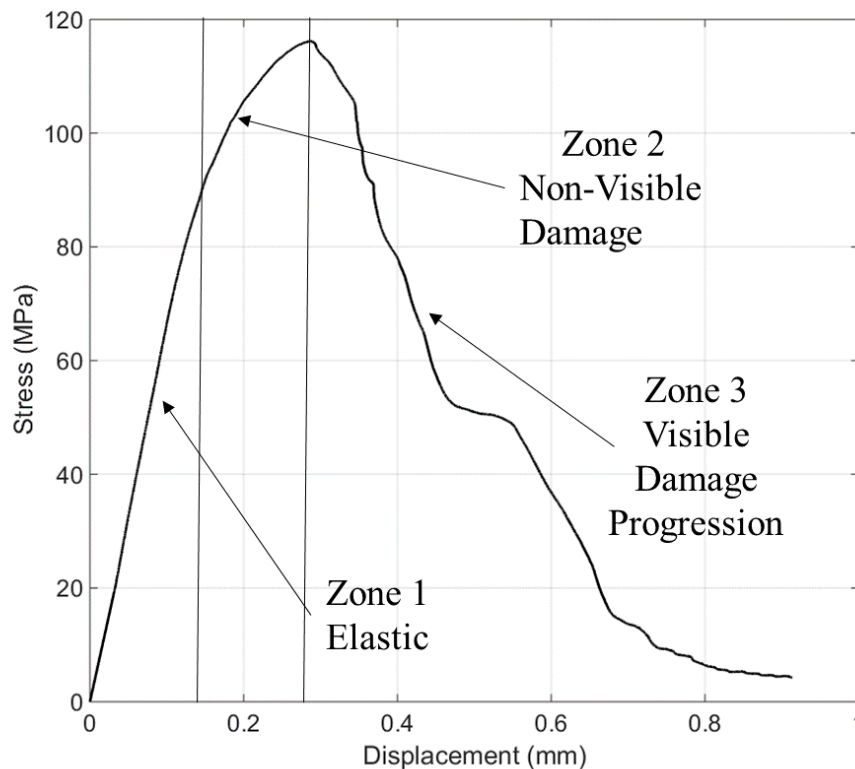
Figure 3-9: Stress-displacement curve of a specimen showing total stiffness degradation due to advancement of damage

In zone 1 of figure 3-9, the stress increases linearly showing elasticity. If the specimen is unloaded in this region it retraces the loading curve back to zero. Zone 2 represents the curve beginning to show non-linearity due to the onset of non-visible damage such as micro cracks or plasticity. In order to determine the plasticity behavior of the material, several uniform compression specimens were loaded until non-linearity in the stress-strain curve was present, then unloaded to show the deformation offset. Figure 3-10 shows some representative stress-strain curves for the unloading tests.
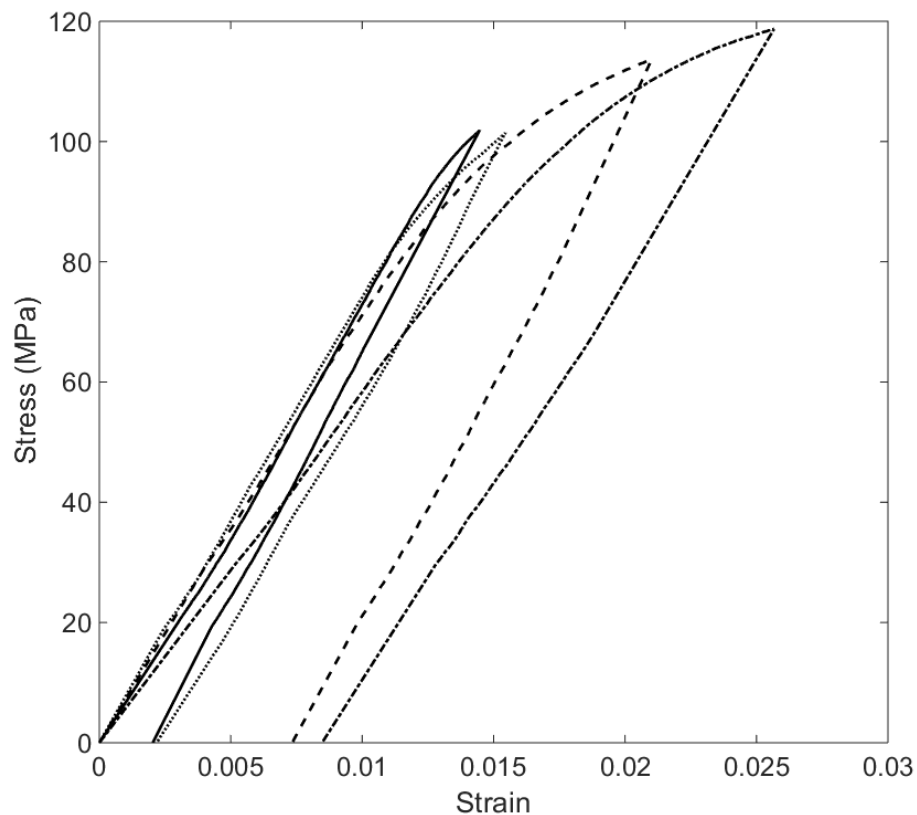
Figure 3-10: Specimen loading curves showing non-linear plasticity

Each specimen shows a non-linear plastic region during the loading. Generally the nonlinearity of the curve begins around a strain of 0.0125. Unloading the specimen in the

non-linear region shows a linear decrease to an offset strain value. Figures 3-10 illustrate that plasticity behavior that is observed in zone 2 of figure 3-9. After the plastic/non-visible damage region, large scale failure of the material begins to occur causing large decreases in stress which is labeled as zone 3 in figure 3-9. Sudden fracture causes a linear decrease in the stress, which is demonstrated by a few of the specimens in figure 8. Figure 3-9 shows slower damage advancement and was able to be loaded monotonically until the stiffness was completely degraded. The slower progression of damage is due to a tortuous crack path causing crack locking and fiber bridging, preventing sudden failure of the entire region.

In all the uniform compression specimens tested, the stress did not instantly degrade to zero after damage occurred. A residual stress was observed that often remained at a consistent level as further displacement was applied which is observed in figures 3-8 and 3-9. Continued loading eventually led to further decrease in stiffness of the material. In addition to the contact of the crack faces and undamaged material, fiber bridging was observed increasing the load carrying ability and the energy dissipation of the damage region. A specimen was re-loaded after fracture occurred to test the post-damage stiffness and continued load carrying ability of the specimen. The specimen selected for reloading showed a uniform shear crack across the specimen and towards the middle of the specimen. A specimen with the crack towards the middle, as in figure 3-7, was selected to ensure that the behavior represented the damaged region instead of loading an undamaged edge of material. Stress displacement data for the damaged specimen is shown in figure 3-11. The stress was calculated using the force over area, so

it does not reflect the true stress in the material. It does reflect a value that could be useful for modeling the specimen damage propagation behavior.
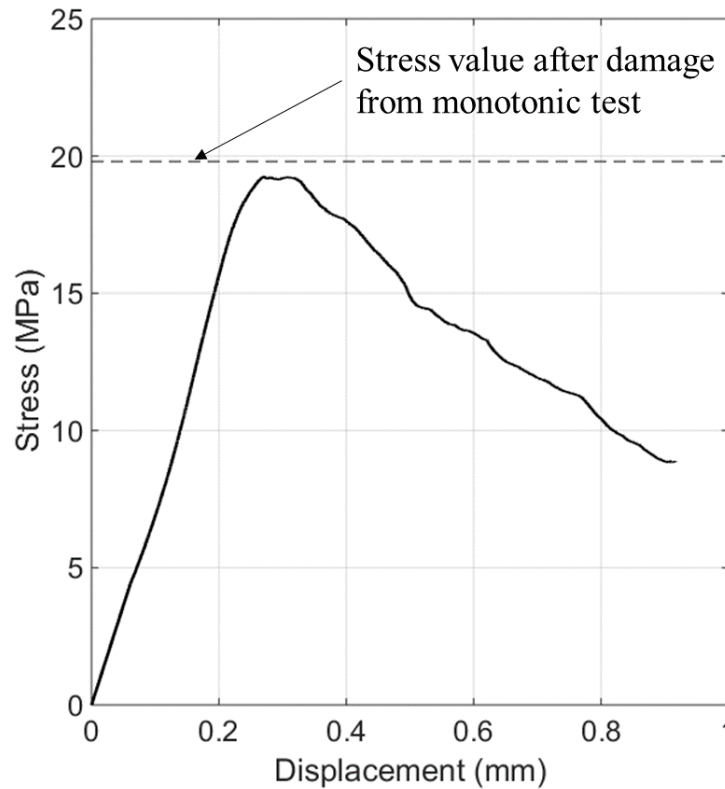
Figure 3-11: Re-loading stress-displacement curve after damage showing the stress value after damage from the monotonic loading tests

The damaged material showed residual stiffness with a linear stress-displacement increase up until around the residual stress values observed in figure 3-8. The stress value holds at the peak through continued displacement, then begins to slowly degrade. Fiber bridging and material locking in the shear crack prevents the crack faces from sliding apart quickly and causing instant degradation of stiffness. These mechanisms combine with crack face friction and contact stresses to allow the material to continue to carry load despite damage. As the fiber bridges break, the faces are able to slide apart causing the

load carrying ability to decrease and the material stiffness to degrade. Eventually the crack faces will slide past each other leading to total degradation of the material. However, total degradation of the material stiffness is not realistic in a conventional laminate as undamaged material ahead of the damage region or other plies in multi-directional laminates create constraints on the material that are not present in the uniform specimens. Constraints prevent the crack faces from sliding completely out of contact causing complete material degradation.

A useful metric for quantifying the damage behavior is the area under the stress displacement curve. This is used as the strain energy release rate in damage mechanics models. The stress-displacement values show a wide spread in figure 8, which leads to varied energy dissipation values. Based on the failure mechanisms observed, the toughness values should vary depending on the fracture plane angle of the shear crack. The area under the curve vs the fracture plane angle is plotted in figure 3-12.
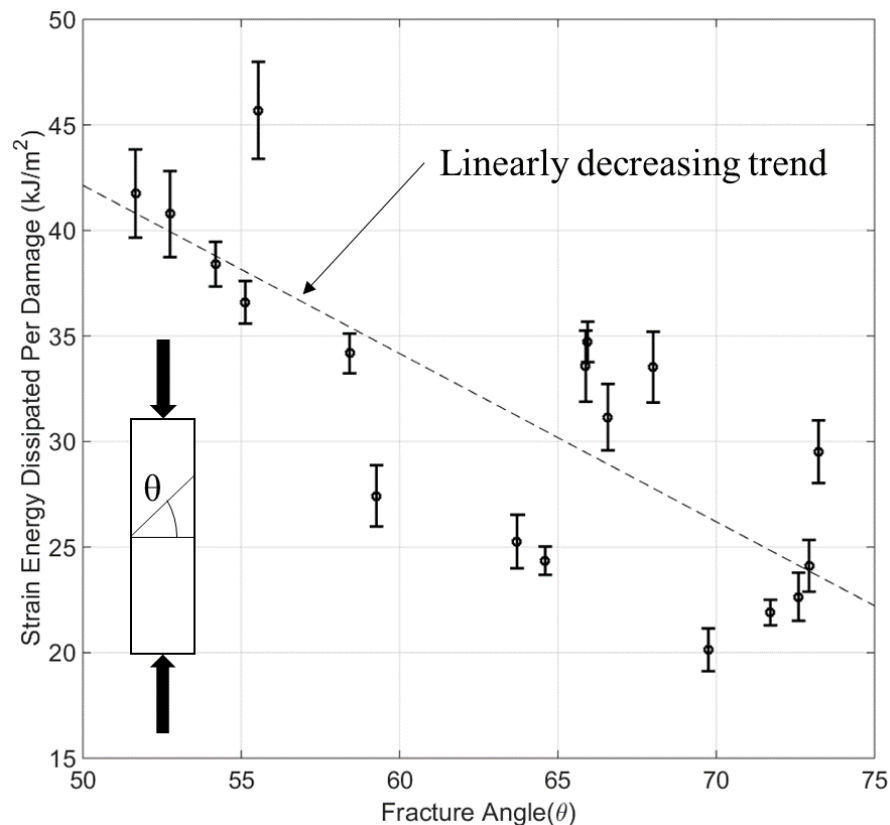
Figure 3-12: Energy dissipated due to damage (as calculated from the area under the strain-displacement curve) versus the fracture plane angle (θ) of the shear crack. Inset shows orientation of fracture angle and loading

Figure 3-12 shows a strong correlation between the energy dissipated and the fracture

plane angle of the material. The energy dissipation rate decreases as the fracture angle

increases. A correlation was not observed in the max stress values or the specimen

geometry, showing that the variation is primarily due to fracture plane changes. This is

consistent with the predictions of Maimi et al. [13]. The dissipation should trend toward

the through thickness mode II strain energy release rate of the material. However, the

measured release rate values are higher than is reported for similar materials using the

mode II energy release rate. This is due to crack face contact, plasticity, fiber bridging,

and material locking that is not taken into account in assumption of a simple mode II crack at an angle. In addition, work by Parmigiani and Thouless [33] showed that in mixed mode loading cases as compressive mode I force increases the fracture toughness of the material. The results of figure 3-12 reflect this, as the compressive mode I force decreases as the fracture plane increases. The four data points between fracture angles of 65° and 68° and the data point at the end, (fracture angle of 73.23°) were specimens that showed multiple failure modes and tortuous crack paths leading to abnormally high toughness values for the respective crack angles. The toughness values vary greatly with the fracture plane angle, ranging from about 46 kJ/m^2 to around 21 kJ/m^2. The largest value of 46 kJ/m^2 corresponded to the specimen that showed complete stiffness degradation shown in figure 3-12. A large sensitivity of the damage energy dissipation to the fracture angle makes modeling the stress displacement behavior difficult with explicitly determining the fracture plane angle.

3.3.2 Compact Compression Specimens

3.3.2.1. Damage Mechanisms

Similar failure mechanisms were observed in the CC specimens as the uniform compression specimens. Shear cracks formed at the notch tip and progressed through the thickness direction at a fracture angle. The cracks were measure to be at angles between 47° and 54° with an average of 50.6°. As the cracks propagate, other damage mechanisms begin to become present. Evidence of delamination of plies was present in some of the specimens where the cracks turn and propagate vertically. This was primarily due to the

interaction of shear cracks, e.g. two shear cracks on the same face creating a wedge that

created a delamination as compression load is applied. A similar mode was predicted

Puck and Schurman [9], which they labeled as Mode C. The multiple failure mechanisms

occurring during the propagation of matrix compression damage is a form of

fragmentation damage described by Matzenmiller et al [34]. It was stated that this is

common in epoxy composite matrices.

In addition to the through thickness propagation, the damage propagated in a

direction parallel to the notch. The notch direction propagation is illustrated in figure 3-

13. This adds additional complexity to the damage mechanisms as the shear cracks are

propagating in to directions simultaneously.
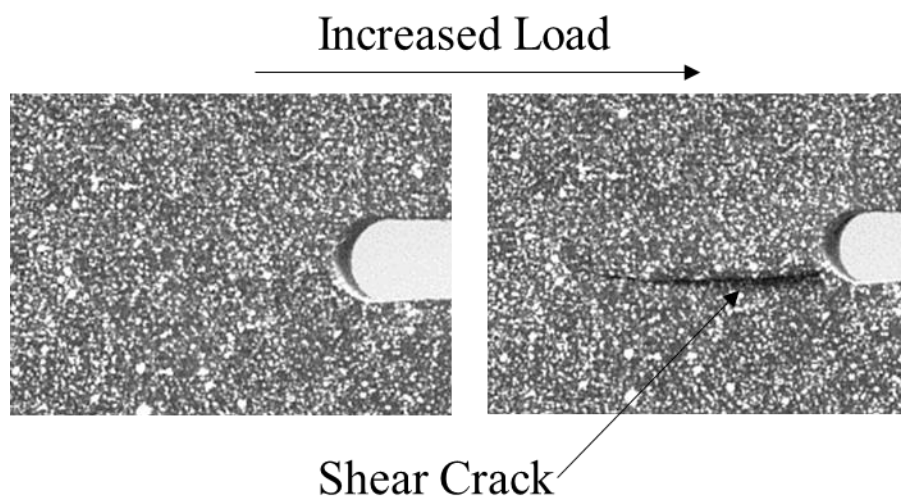
Figure 3-13: Progression of crack parallel to the notch tip taken from DIC images of specimen. The white box highlights the crack growth

In addition, there is a mode II shear crack propagating perpendicular to the notch

direction. This illustrates an undesired failure mode in the specimen. Since figure 3-13 is

taken from the speckle images, the crack is obscured by the speckle images and the

lighting. Figure 3-14 shows an image of a failed specimen showing the two crack propagation directions. Dye penetrant that fluoresces under UV light was used to highlight the crack in the image.
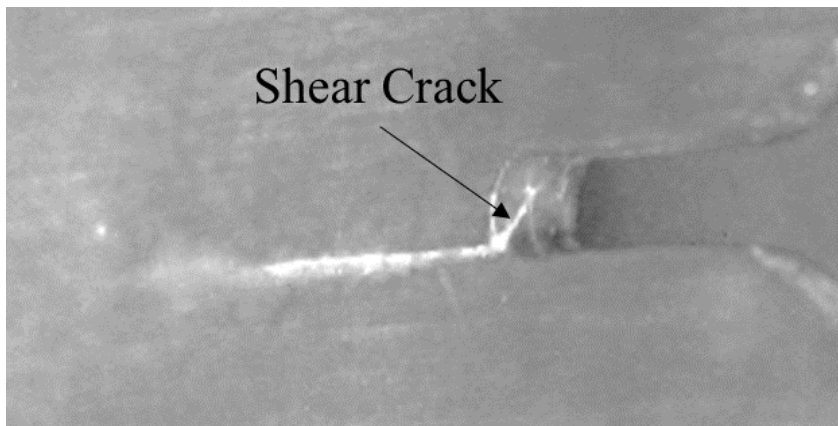
Figure 3-14: Failed specimen showing growth of crack parallel to the notch tip and through the specimen thickness

The final failure in all the specimens tested was tensile failure of the specimen's back end. This is a limitation of CC specimens. A sample after tensile splitting is shown in figure 3-15.
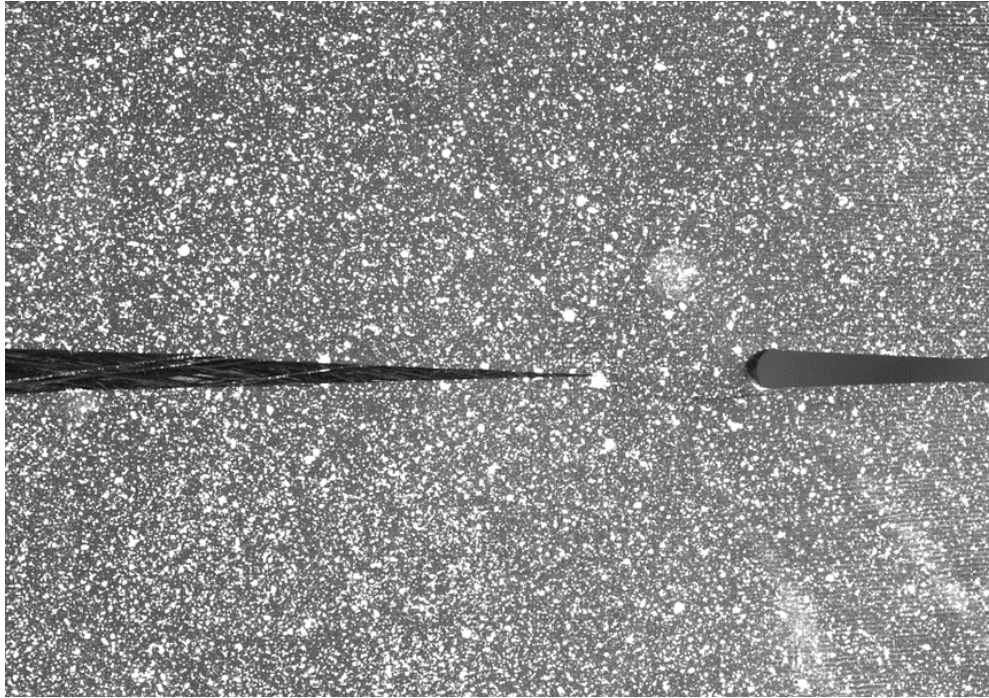
Figure 3-15: Specimen showing final tensile splitting failure of the back end opposite of the notch tip after significant compressive damage propagation occurred

Matrices tend to be stronger in compression than in tension, which is opposite of the fibers. Since the load is applied at one location the notch acts as a fulcrum causing tensile loads in the back end of the specimen. The material works as a closing force, as compression damage progresses the lever arm preventing the splitting shortens creating a large force in the material. Eventually the force creates a stress greater than the tensile strength of the matrix leading to splitting. Tensile splitting can be delayed by extending the length between the notch tip and the back edge of the specimen or applying a clamping force on the back end. Specimens were tested with both a clamping force applied and without. The specimens showed some progression without clamping force, but adding clamping greatly improved the size of the crack before tensile failure.

3.3.2.2. Stress Displacement Curves and Energy Release

The uniform compression experimental results can be used to determine the validity of
the basic J-integral assumptions to the compressive damage region. The J-integral is
derived from an energy balance per unit thickness and a virtual crack extension in a
coordinate direction. Therefore it can be generalized to the energy dissipated per region
of damage growth for compression damage propagation provided the contour avoids the
plastic region and plastic region is relatively small. Figure 3-10 illustrate the plasticity
occurs in the specimen prior to visible damage onset. From the curves, a strain value of
0.0125 is used for the onset of plasticity. The DIC strain fields can be used to determine
the plastic region size. Figure 16 shows the strain field just before damage occurs.
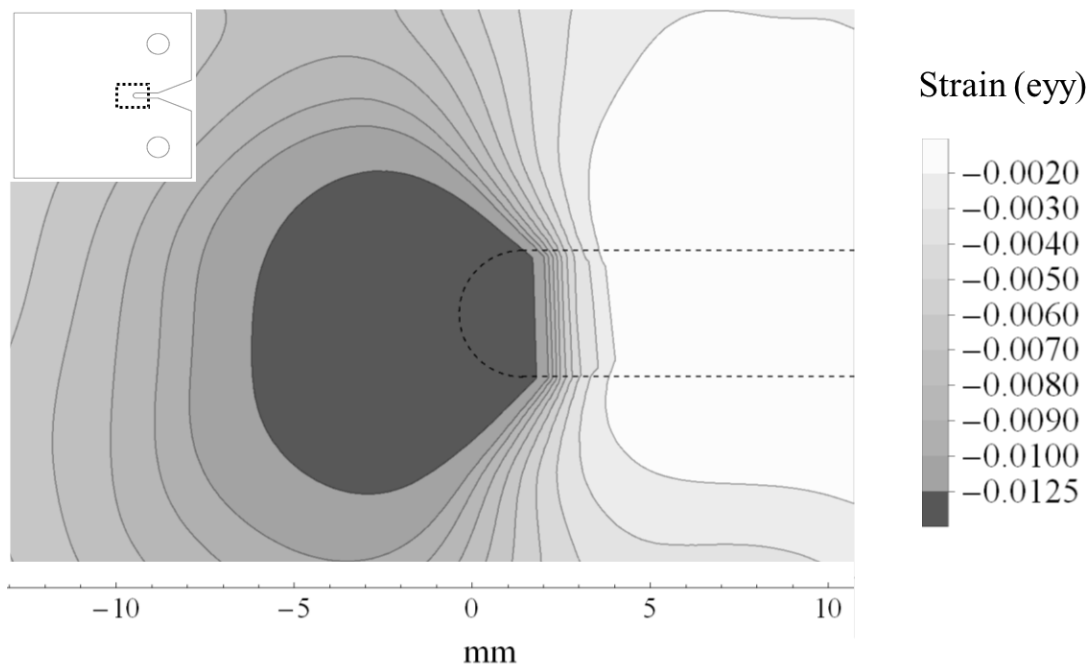
**Figure 3-16: Compressive strain fields showing plastic region size. The dashed line on the specimen
in the upper corner shows the approximate region of the strain field**

In figure 3-16, the dark region represents an estimate of the plastic region based on the measured initiation value from figure 3-10. The contour was selected to avoid this plastic region. The plastic region is much smaller than the ligament length of the specimens. The length of the plastic region is about 7 mm compared to the ligament length of 69.75 mm. The J-integral requires quasi-static and monotonic loading for materials exhibiting plasticity. These conditions were met during the loading of the specimens before damage occurred. Once damage occurs, unloading occurs due to energy dissipation and the displacement control, which may invalidate the J-integral values for damage propagation.

The R-curves calculated from the CC specimen DIC are shown in figure 3-17. Each symbol represents a different CC specimen test.
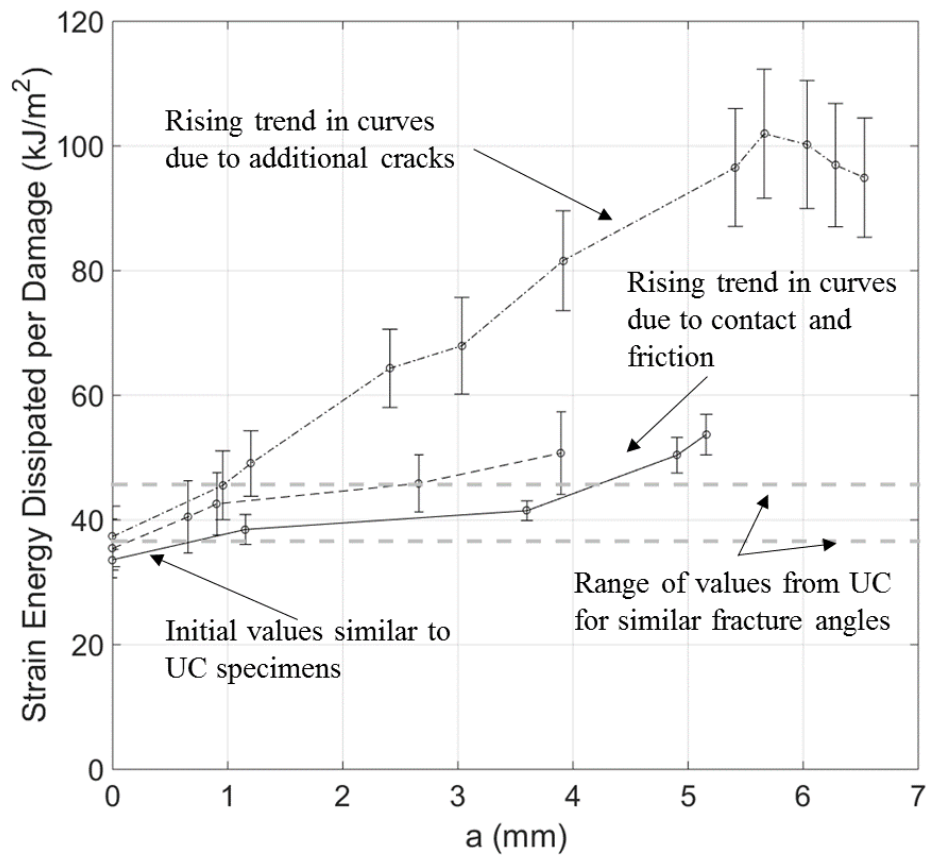
Figure 3-17: Energy dissipated due to damage (as calculated from the area under the strain-displacement curve) versus damage region length (a) with a comparison to the uniform compression (UC) specimens. Each line represents a different CC specimen

The general trend of the energy dissipation curve shows the value increasing as damage

progression. This is potentially due to several factors. Friction between the crack faces,

contact stresses between the faces, and crushed material trapped inside the damage zone

would cause an increase in energy required to advance the damage zone. These

mechanisms would increase as damage progressed in the specimen and are all consistent

with the observed failure mechanisms in the material. Additionally rising trends in figure

3-17 could be due to different failure mechanism becoming present as the damage

progressed, e.g. a delamination created by shear wedges as observed in some of the specimens. The highest energy dissipation values during damage progression were in a specimen that showed several shear cracks as well as delamination of plies that would cause the J-integral values to increase. This may invalidate the J-integral for propagation of compression damage as new damage and energy dissipation mechanisms may invalidate the energy balance that is the basis of the contour integral. The J-Integral values show a wide spread across different specimens tested. Typical initiation values range from 30 kJ/m^2 to 40 kJ/m^2. The calculated value from the uniform compression specimens falls within the range of calculated values from the J-integral for initiation of damage. Most fall within the range of predicted toughness based on fracture plane angles; 35-40 kJ/m^2 for angles between 50 and 55°. The CC specimen that showed the lowest initiation J-integral value showed initially high fracture plane angles, which is consistent with the results of the uniform compression specimens. It is important to note that the strain energy release rate measured in compression is analogous to the fracture mechanics definition in the sense that it is the energy dissipated per advancement of damage, but the energy dissipated is not purely due to the same mechanisms. In fracture, the energy dissipated is due to new surfaces being created. For compression, there are many more potential energy dissipation mechanisms such as frictional contact. Due to the spread of the values and the increasing trends further techniques are required to classify the damage propagation behavior.

Commonly the stress displacement behavior is used in damage mechanics models. Therefore it is important to classify this behavior to determine appropriate models. A

potential method is to use the DIC field data from the CC specimens to create elements that surrounds the damage region and measure the stress displacement behavior of that element. The stress value should be accurate as long as the points chosen are sufficiently far from the damage region. The drawback of this method is that the stress displacement law is highly dependent on the distance from the damage region tip because of the notch stress singularity and the sharp stress gradient. Therefore, this method is only useful for qualitatively measuring the behavior of the damage region or using it as a metric for potential models. Figure 3-18 shows the stress displacement behavior of a representative element above a damage zone in a CC specimen.
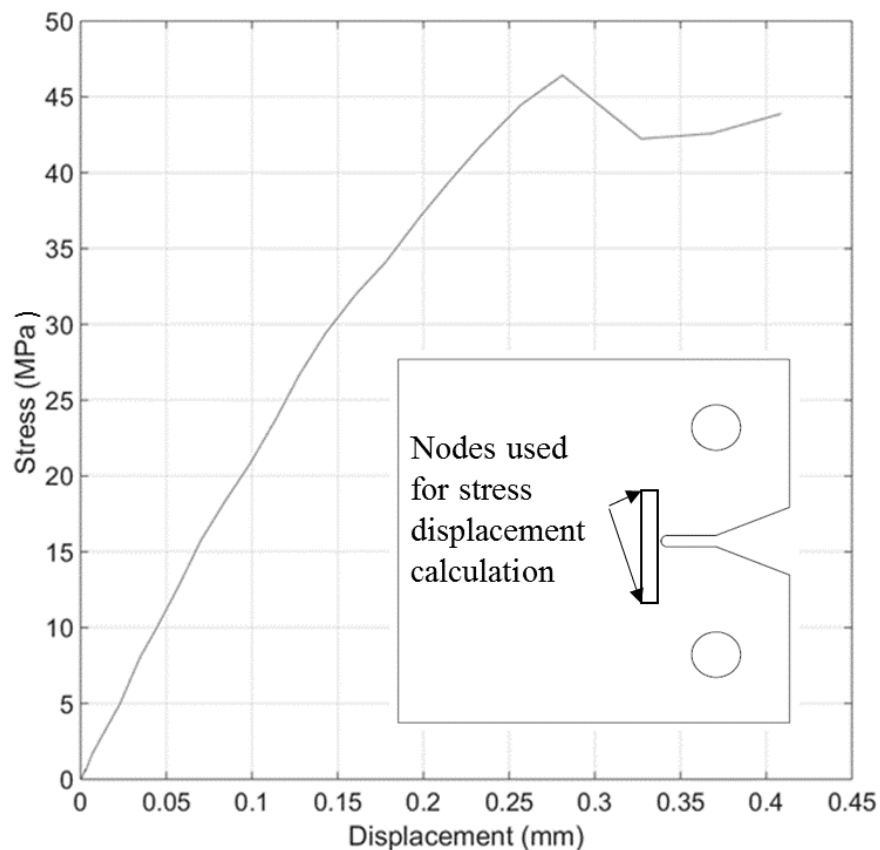
Figure 3-18: Stress displacement behavior of an element encompassing the damage region

Figure 3-18 illustrates a deviation from a bilinear continuum damage mechanics model.

The continuum damage mechanics model predicts continued degradation of the material

stiffness. A similar plot for a continuum damage mechanics model shows the stiffness

degrading linearly until zero. Figure 3-19 shows the stress begin to increase after the

initial drop off. Based on the observed failure mechanisms, this is potentially a result of

the contact between the crack faces. This effect is amplified for the damage progression

case because the undamaged material at the crack tip prevents the faces from sliding past

each other quickly. In addition, undamaged material in the damage region carries some

additional load. The stress-displacement behavior of the elements change when moving

away from the notch tip along the damage zone. This change is shown in figure 3-19 with

each line representing a different x distance from the notch tip.
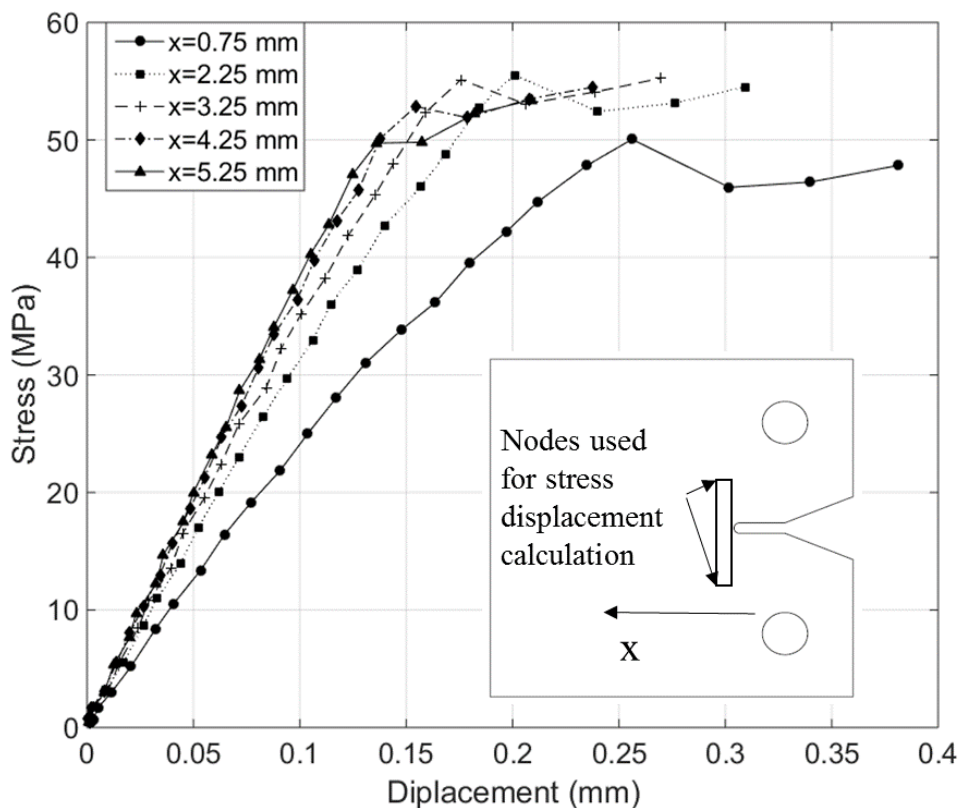
Figure 3-19: Stress-Displacement behavior of DIC test elements showing variation in the x direction

The trend shown in figure 3-18 is reflected in figure 3-19 for many of the elements. The

changes in the trends and values is caused by shifts in the damage region changing the

singularity fields, as well as crack face contact changing along the damage region.

3.4   Conclusion

Experimental techniques were used to classify the matrix compression damage

propagation behavior in carbon fiber/epoxy composites. CC specimens were used to

isolate the damage and force propagation in a desired direction. Shear cracks through the thickness of the material were shown to be the primary failure mechanisms present in the specimens. Other failure mechanisms were observed in the specimens as damage progressed further due to interaction of damage. The damage was also shown to propagate in the direction parallel to the notch direction as desired. However, the progression was limited because the back end of the specimen tended to fail in tension. This is a limit of the CC specimens, but design of the specimens and the fixtures can delay the onset of this damage. Specimens can be modified to extend the distance between the notch tip and the back end delaying tensile failure. Clamps can be used to prevent the splitting. J-integral calculations were used to determine the energy dissipation rate per advancement of damage region. The results showed increasing R-curve trends caused by crack face contact, friction, fiber bridging, and undamaged material trapped in the wake of the damage region. Stress-displacement behavior of elements surrounding the notch tip showed continued load carrying capability of the material after damage. Uniform compression specimens were used to further classify the stress displacement behavior of damage. Failure in these specimens usually occurred to quickly to measure the full progression of damage; however these specimens revealed several key behaviors. The specimens showed a residual stress carrying ability after damage and reloading specimens showed the residual stiffness behavior. Plasticity was observed in the specimens just before damage. Complete failure only occurred when damage the crack faces slipped past each other and were no longer in contact. Plotting the area under these stress-displacement curves showed a strong correlation with fracture angle. This trend is

predicted in the literature. The area under the stress-displacement curves agreed fairly well with the initiation J-integral values. The results of matrix compression damage propagation experiments showed complex behavior that is not predicted by simple bi-linear energy release rate models. The energy dissipated varies greatly depending on damage propagation, fracture angle, and energy dissipation mechanisms present in the damage region. More detailed models are required to accurately capture the damage behavior. More work is required on the contribution of each component of damage (e.g. fracture, fiber bridging, friction, contact stresses) to the energy release rate and other metrics.

3.5 References

[1] B. Budiansky, "Micromechanics," *Computers and Structures,* vol. 16, pp. 3-12, 1983.

[2] N. Fleck, P. Jelf and P. curtis, "Compressive Failure of Laminated and Woven Composited," *Journal of Composites Technology and Reseach,* vol. 17, no. 3, pp. 212-220, 1995.

[3] A. Argon, "Fracture of Compsites," *Treatise ofMaterial Science and Technology ,* vol. 1, 1972.

[4] P. M. Jelf and N. A. Fleck, "Compression Failure Mechanisms in Unidirectional Composites," *Journal of Composite Materials,* vol. 26, pp. 2706-2728, 1992.

[5] S. Narayanan and L. S. Schadler, "Mechanisms of kink-band formation in graphite/epoxy composites: a micromechanical experimental study," *Composites Science and Technology,* vol. 59, no. 15, p. 2201–2213, 1999.

[6] C. Soutis and P. Curtis, "A method for predicting the fracture toughness of CFRP laminates failing by fibre microbuckling," *Composites Part A: Applied Science and Manufacturing,* vol. 31, no. 7, pp. 733-740, 2000.

[7] C. G. DAVILA, P. P. CAMANHO and C. A. ROSE, "Failure Criteria for FRP Laminates," *Journal of Composite Materials,* vol. 39, no. 4, 2005.

[8] C. Gonzalez and J. LLorca, "Mechanical behavior of unidirectional fiber-reinforced polymers under transverse compression: Microscopic mechanisms and modeling," *Composites Science and Technology,* vol. 67, no. 13, p. 2795–2806, 2007.

[9] A. Puck and H. Schurmann, "Failure analysis of FRP Laminates by means of physically based phenomenlogical models," *Composites Science and Technology,* vol. 58, pp. 1045-1067, 1998.

[10] R. M. Christensen and S. J. DeTeresa, "Failure plane orientations for transverse loading of a unidirectional fiber composite," *International Journal of Solids and Structures ,* vol. 40, pp. 7055-7062, 2003.

[11] S. T. Pinho, C. G. Davila, P. P. Camanho, L. Iannucci and P. Robinson, "Failure Models and Criteria for FRP Under In-Plane or Three-Dimensional Stress States Including Shear Non-Linearity," NASA/TM-2005-213530, 2005.

[12] S. Pinho, P. Robinson and L. Ianucci, "Fracture toughness of the tensile and compressive fibre failure modes in laminated composite," *Composites Science and Technology,* vol. 66, pp. 2069-2079, 2006.

[13] P. Maimi, P. P. Camanho, J.-A. Mayugo and C. G. Davila, "A Thermodynamically Consistent Damage Model for Advanced Composites," NASA/TM-2006-214282, 2006.

[14] P. Maimi, P. Camanho, J. Mayugo and C. Davila, "A continuum model for composite laminates: Part I-Constituitive Model," *Mechanics of Materials,* vol. 39, pp. 897-908, 2007.

[15] I. Lapczyk and J. A. Hurtado, "Progressive damage modeling in fiber-reinforced materials," *Composites Part A: Applied Science and Manufacturing,* vol. 38, pp. 2333-2341, 2007.

[16] Z. O. Bazant and B. Oh, "Crack band theory for the fracture of concrete," *Materials and Structures,* vol. 16, pp. 155-177, 1983.

[17] M. Sutcliffe and N. Fleck, "Mirobuckle Propagation in Fibre Composites," *Acta Mateallurgica et Materilia,* vol. 42, pp. 2219-2231, 1994.

[18] R. S. Vaidya and C. Sun, "Fracture Criterion for Notched Thin Composite Laminates," *AIAA Journal,* vol. 35, no. 2, pp. 311-316, 1997.

[19] Y. Yeow, D. Morris and Y. Brinson, "A correlaive study between analysis and experiment on the fracture behavior of graphit/epoxy composites," *Journal of testing and evaluation,* vol. 7, no. 2, pp. 117-125, 1979.

[20] ASTM, *E399-06 Standard Test Method for Linear-Elastic Plane-Strain Fracture Toughness KIc of Metallic Materials,* 2006.

[21] J. Ratcliffe, W. Jackson and J. Schaff, "Compression Strength Prediction of Impact-Damaged Composite Sandwich Panels," in *60th Annual Forum Proceedings, American Helicopter Society*, Baltimore, 2004.

[22] G. Catalanotti, P. Cmanho, J. Xavier, C. Davila and A. Marques, "Measurement of resistance curves in the logitudinal failure of composites using digital image correlation," *Composites Science and Technology,* vol. 70, pp. 1986-1993, 2010.

[23] S. Pinho, P. Robinson and I. Iannucci, "Developing a four point bend specimen to measure the mode I intrlaminar frature toughness of unidirection laminated composites," *Composites Science and Technology,* vol. 69, pp. 1303-1309, 2009.

[24] M. Laffan, S. Pinho, P. Robinson, L. Iannuci and A. McMillan, "Measurement of the fracture toughess associated with the longitudinal fibre compressive failure mode of laminated composites," *Composites: Part A,* vol. 43, pp. 1930-1938, 2012.

[25] M. Laffan, S. Pinho, P. Robinson and A. Mcmillan, "Translaminar fracture toughness testing of composites: A review," *Polymer Testing,* vol. 31, pp. 481-489, 2012.

[26] M. Laffan, S. Pinho, P. Robinson and L. Iannucci, "Measurement of the in sity ply fracture toughness associated with mode I fibre tensile failure in FRP. Part I: Data Reduction," *Composites Science and Technology,* vol. 70, pp. 606-613, 2010.

[27] M. Kortschort and P. Beaumont, "Damage Mechanics of Composite Materials: I-Measuremnets of Damage and Strength," *Composites Science and Technology,* vol. 39, pp. 289-301, 1990.

[28] C. Harris and D. Morris, "Fracture Behavior of Thick, Laminated Graphite/Epoxy Composites, Nasa Contractor Report 3784," 1984.

[29] J. Arby, S. Bochard, A. Chateauminois, M. Salvia and G. Giraud, "In situ detection of damage in CFRP llaminates by electrical resistance mthods," *Composites Science and Technology,* vol. 59, pp. 925-935, 1999.

[30] R. Reber, J. De Haan, J. Mayer, M. Petitmermet and E. Wintermatnel, "Intralaminar Fracture of Weft-Knitted Carbon Fiber Reinforced PEEK," *European Structural Integrity Society,* vol. 27, p. 123–133, 2000.

[31] M. A. Daniels, T. Rawlings and J. P. Parmigiani, "Selection and Validation of Experimenal Specimens for Determining Model Inputs for Matrix Compression

Damage Propagation in Fiber Reinforced Composites," in *Proceedings of the ASME 2016 International Mechanical Engineering Congress & Exposition*, Phoenix, AZ, 2016.

[32] J. Rice, "A Path Independent Integral and Approximate Analysis of Strain Concentration by Notches and Cracks," *Journal of Applied Mechanics,* vol. 16, pp. 13-31, 1968.

[33] J. Parmigiani and M. Thouless, "The effects of cohesive strength and toughness on mixed-mode delamination of beam-like geometries," *Engineering Fracture Mechanics,* vol. 74, no. 17, pp. 2675-2699, 2007.

[34] A. Matzemiller, J. Lubliner and R. Taylor, "A constitutive model for anisotropic damage in fiber-composites," *Mechanics of Materials ,* vol. 20, pp. 125-152, 1995.

[35] A. Parvizi, K. Garret and B. J. E., "Constrained cracking in glass fiber reinforced epoxy cross-ply laminates," *Journal of Material Science,* vol. 13, pp. 195-201, 1978.

CHAPTER 4: GENERAL CONCLUSION

This investigation sought to experimentally determine the mechanisms and behavior of matrix compression damage propagation in carbon fiber composites. The first study focused on determining an appropriate specimen to achieve matrix compression damage reliably. Then, experimental specimens were used to classify the mechanical behavior matrix compression damage propagation.

Candidate specimens were determined from literature on compression damage in composite materials. The specimens considered were CNC specimens, CC specimens, and 4PB specimens. These specimens were modelled using finite element analysis and the size of the predicted damage region was used to compare the specimens. 4PB specimens showed primarily tensile failure of the end opposite of the notch. CC and CNC specimens both showed good isolation of compression damage in the models. However, the damage modes in CNC specimens were highly dependent on the boundary conditions used in the models. In order to remove fixture dependence, CC specimens were selected for further study. Sample CC specimens were manufactured and tested to verify the concept. These specimens showed good isolation of compression damage without global buckling.

Once the specimens were selected and tested, the manufacturing techniques and data collection techniques were refined to determine the compressive damage propagation behavior in the matrix. DIC was used to measure the displacement and strain fields. The J-integral and stress-displacement behavior of damaged material were used to

classify the effect of damage. In addition to the CC specimens, uniform compression specimens were used to measure the stress-displacement behavior without a strain concentration. Shear cracks through the thickness of the material were the dominate failure mechanism observed in all the specimens tested. After propagation of damage began, other failure mechanisms, such as ply delamination, were observed. The J-integral curves showed an increasing trend due to contact stresses, crack locking, crack friction, and trapped undamaged material increasing as damage progresses clouding the energy dissipation values. The stress-displacement behavior of the CC specimens showed an increasing load after damage that is caused by similar mechanisms. Uniform stress-displacement curves showed similar residual loads and revealed fiber bridging as another mechanism. These curves also showed plasticity in the material before crack propagation. The area under the uniform stress displacement curves showed the material toughness is highly dependent on the fracture plane angle of the shear cracks. Results from the experimental study show that matrix compression damage is complex and may not be accurately represented by common models.

The studies presented here reveal the importance of experimental classification of damage. Matrix compression damage is complex and dependent on several mechanisms that are not accounted for in simple, commonly used models. It is difficult to determine a single input that would capture the full behavior of the observed damage. A basic model needs to account for fractured angle effects and the residual load carrying abilities. More refined models could account for friction, crack contact and fiber bridging separately.

CC specimens were selected in the first study and used extensively in the second study. These specimens demonstrated the ability to isolate matrix compression damage. However, there are some limitations of these specimens. Composite matrices are typically weaker in tension then compressions causing the CC specimens to ultimately fail in tension after some compression damage propagation. This can be delayed by extending the dimension between the notch tip and the specimen back edge or applying a closing force on the specimen back end. The observed behavior makes it difficult to capture the damage behavior with a single input parameter measured from CC specimens. Further study with different specimens is required to determine the effects of each mechanism (e.g. shear crack propagation, crack friction, etc.) to the damage propagation. CC specimens are a useful metric for models because of their isolation of the desired failure modes.

CHAPTER 5: BIBLIOGRAPHY

[1] A. Puck and H. Schurmann, "Failure analysis of FRP Laminates by means of physically based phenomenlogical models," *Composites Science and Technology,* vol. 58, pp. 1045-1067, 1998.

[2] R. M. Christensen and S. J. DeTeresa, "Failure plane orientations for transverse loading of a unidirectional fiber composite," *International Journal of Solids and Structures ,* vol. 40, pp. 7055-7062, 2003.

[3] S. T. Pinho, C. G. Davila, P. P. Camanho, L. Iannucci and P. Robinson, "Failure Models and Criteria for FRP Under In-Plane or Three-Dimensional Stress States Including Shear Non-Linearity," NASA/TM-2005-213530, 2005.

[4] P. M. Jelf and N. A. Fleck, "Compression Failure Mechanisms in Unidirectional Composites," *Journal of Composite Materials,* vol. 26, pp. 2706-2728, 1992.

[5] A. Argon, "Fracture of Compsites," *Treatise ofMaterial Science and Technology ,* vol. 1, 1972.

[6] B. Budiansky, "Micromechanics," *Computers and Structures,* vol. 16, pp. 3-12, 1983.

[7] N. Fleck, P. Jelf and P. curtis, "Compressive Failure of Laminated and Woven Composited," *Journal of Composites Technology and Reseach,* vol. 17, no. 3, pp. 212-220, 1995.

[8] S. Narayanan and L. S. Schadler, "Mechanisms of kink-band formation in graphite/epoxy composites: a micromechanical experimental study," *Composites Science and Technology,* vol. 59, no. 15, p. 2201–2213, 1999.

[9] C. Soutis and P. Curtis, "A method for predicting the fracture toughness of CFRP laminates failing by fibre microbuckling," *Composites Part A: Applied Science and Manufacturing,* vol. 31, no. 7, pp. 733-740, 2000.

[10] S. Pinho, P. Robinson and L. Ianucci, "Fracture toughness of the tensile and compressive fibre failure modes in laminated composite," *Composites Science and Technology,* vol. 66, pp. 2069-2079, 2006.

[11] P. Maimi, P. Camanho, J. Mayugo and C. Davila, "A continuum model for composite laminates: Part I-Constituitive Model," *Mechanics of Materials,* vol. 39, pp. 897-908, 2007.

[12] I. Lapczyk and J. A. Hurtado, "Progressive damage modeling in fiber-reinforced materials," *Composites Part A: Applied Science and Manufacturing,* vol. 38, pp. 2333-2341, 2007.

[13] Z. O. Bazant and B. Oh, "Crack band theory for the fracture of concrete," *Materials and Structures,* vol. 16, pp. 155-177, 1983.

[14] J. Aveston and A. Kelly, "Theory of multiple fracture of fiberous composites," *Journal of Material Science,* vol. 8, pp. 352-362, 1973.

[15] Y. Han, H. Hahn and R. Croman, " A simplified analysis of transverse ply cracking in cross-ply," *Composites science and Technology,* vol. 31, pp. 165-177, 1988.

[16] P. Maimi, P. Camanho, J. Mayugo and A. Turon, "Matrix cracking and delamination in laminated composites. Part I: Ply constitutive law, first ply failure and onset of delamination," *Mechanics of Materials,* vol. 43, pp. 169-185, 2011.

[17] C. G. DAVILA, P. P. CAMANHO and C. A. ROSE, "Failure Criteria for FRP Laminates," *Journal of Composite Materials,* vol. 39, no. 4, 2005.

[18] C. Gonzalez and J. LLorca, "Mechanical behavior of unidirectional fiber-reinforced polymers under transverse compression: Microscopic mechanisms and modeling," *Composites Science and Technology,* vol. 67, no. 13, p. 2795–2806, 2007.

[19] M. Sutcliffe and N. Fleck, "Mirobuckle Propagation in Fibre Composites," *Acta Mateallurgica et Materilia,* vol. 42, pp. 2219-2231, 1994.

[20] R. S. Vaidya and C. Sun, "Fracture Criterion for Notched Thin Composite Laminates," *AIAA Journal,* vol. 35, no. 2, pp. 311-316, 1997.

[21] Y. Yeow, D. Morris and Y. Brinson, "A correlaive study between analysis and experiment on the fracture behavior of graphit/epoxy composites," *Journal of testing and evaluation,* vol. 7, no. 2, pp. 117-125, 1979.

[22] The Boeing Co., ""Advanced Composite Compression Tests", Boeing Specification Support Standard BSS 7260, Rev. C," The Boeing Co., Seattle Washington, 1988.

[23] J. Ratcliffe, W. Jackson and J. Schaff, "Compression Strength Prediction of Impact-Damaged Composite Sandwich Panels," in *60th Annual Forum Proceedings, American Helicopter Society*, Baltimore, 2004.

[24] G. Catalanotti, P. Cmanho, J. Xavier, C. Davila and A. Marques, "Measurement of resistance curves in the logitudinal failure of composites using digital image correlation," *Composites Science and Technology,* vol. 70, pp. 1986-1993, 2010.

[25] ASTM, *E399-06 Standard Test Method for Linear-Elastic Plane-Strain Fracture Toughness KIc of Metallic Materials,* 2006.

[26] S. Pinho, P. Robinson and I. Iannucci, "Developing a four point bend specimen to measure the mode I intrlaminar frature toughness of unidirection laminated composites," *Composites Science and Technology,* vol. 69, pp. 1303-1309, 2009.

[27] M. Laffan, S. Pinho, P. Robinson, L. Iannuci and A. McMillan, "Measurement of the fracture toughess associated with the longitudinal fibre compressive failure mode of laminated composites," *Composites: Part A,* vol. 43, pp. 1930-1938, 2012.

[28] M. Laffan, S. Pinho, P. Robinson and A. Mcmillan, "Translaminar fracture toughness testing of composites: A review," *Polymer Testing,* vol. 31, pp. 481-489, 2012.

[29] M. Laffan, S. Pinho, P. Robinson and L. Iannucci, "Measurement of the in sity ply fracture toughness associated with mode I fibre tensile failure in FRP. Part I: Data Reduction," *Composites Science and Technology,* vol. 70, pp. 606-613, 2010.

[30] M. Kortschort and P. Beaumont, "Damage Mechanics of Composite Materials: I-Measuremnets of Damage and Strength," *Composites Science and Technology,* vol. 39, pp. 289-301, 1990.

[31] C. Harris and D. Morris, "Fracture Behavior of Thick, Laminated Graphite/Epoxy Composites, Nasa Contractor Report 3784," 1984.

[32] J. Arby, S. Bochard, A. Chateauminois, M. Salvia and G. Giraud, "In situ detection of damage in CFRP llaminates by electrical resistance mthods," *Composites Science and Technology,* vol. 59, pp. 925-935, 1999.

[33] R. Reber, J. De Haan, J. Mayer, M. Petitmermet and E. Wintermatnel, "Intralaminar Fracture of Weft-Knitted Carbon Fiber Reinforced PEEK," *European Structural Integrity Society,* vol. 27, p. 123–133, 2000.

[34] J. Rice, "A Path Independent Integral and Approximate Analysis of Strain Concentration by Notches and Cracks," *Journal of Applied Mechanics,* vol. 16, pp. 13-31, 1968.

[35] P. Maimi, P. P. Camanho, J.-A. Mayugo and C. G. Davila, "A Thermodynamically Consistent Damage Model for Advanced Composites," NASA/TM-2006-214282, 2006.

[36] A. Matzemiller, J. Lubliner and R. Taylor, "A constitutive model for anisotropic damage in fiber-composites," *Mechanics of Materials ,* vol. 20, pp. 125-152, 1995.

[37] M. A. Daniels, T. Rawlings and J. P. Parmigiani, "Selection and Validation of Experimenal Specimens for Determining Model Inputs for Matrix Compression Damage Propagation in Fiber Reinforced Composites," in *Proceedings of the ASME 2016 International Mechanical Engineering Congress & Exposition*, Phoenix, AZ, 2016.

[38] J. Parmigiani and M. Thouless, "The effects of cohesive strength and toughness on mixed-mode delamination of beam-like geometries," *Engineering Fracture Mechanics,* vol. 74, no. 17, pp. 2675-2699, 2007.